5-1-2021

Characterizing of Monoamine Neurotransmitters at the Hub of the Central Auditory System

Patrick Wilson
University of Northern Colorado

Follow this and additional works at: https://digscholarship.unco.edu/theses

UNIVERSITY OF NORTHERN COLORADO

Greeley, Colorado

The Graduate School

CHARACTERIZING OF MONOAMINE NEUROTRANSMITTERS AT THE HUB OF THE CENTRAL AUDITORY SYSTEM

A Thesis Submitted in Partial Fulfillment
Of the Requirements for the Degree of
Master of Science

Patrick Wilson

College of Natural and Health Sciences
Department of Chemistry and Biochemistry

May 2021

This Thesis by: Patrick Wilson

Entitled: Characterizing of Monoamine Neurotransmitters at the Hub of the Central Auditory System

has been approved as meeting the requirement for the Degree of Master of Science in College of Natural and Health Sciences in School or Department of Chemistry and Biochemistry, Program of Master of Science in Chemistry.

 Accepted by the Thesis Committee:

_____

Aaron K. Apawu, Ph.D., Advisor

_____

Hua Zhao, Ph.D., Committee Member

_____

Robert Houser, Ph.D., Committee Member

Accepted by the Graduate School

_____

Jeri-Anne Lyons, Ph.D.
Dean of the Graduate School
Associate Vice President of Research

ABSTRACT

Wilson, Patrick. *Characterizing of Monoamine Neurotransmitters at the Hub of the Central Auditory System*. Unpublished Master of Science thesis, University of Northern Colorado, 2021.

In the United States, loss of hearing impacts approximately 48.1 million people. The cumulative effects of noise are experienced in every area of society whether occupational, environmental, or through aging. A number of studies have linked noise induced hearing disorders to changes in spontaneous neuronal activity in certain auditory brain regions, especially, the inferior colliculus, a region that integrates auditory inputs from both ascending and descending pathways. However, the exact neurochemical basis of these disorders remains elusive. Currently, there are several compelling pieces of evidence that implicate the monoamine neurotransmitter, dopamine, in auditory processing. Based on this data, we have hypothesized that changes in the dopamine system within the inferior colliculus would contribute to the neural dysfunction underlining noise induced hearing loss. To examine this hypothesis, 32 Adult Sprague Dawley rats were used. The present work optimized a fast scan cyclic voltammetry (FSCV) assay and used it to characterize the dopamine system in rat brain, then examined the impact of loud noise on the system and finally, explore possible mechanisms underlying noise induced changes in the system. The FSCV assay provided the speed, selectivity, sensitivity, and the spatial resolution needed for the neurochemical measurement. The assay also allowed simultaneous detection and monitoring of both dopamine and another monoamine, norepinephrine in the inferior colliculus for the first time. These signals were pharmacologically

confirmed and were found to be significantly and simultaneously attenuated by exposure to loud noise that has been characterized to cause permanent deafness. This data suggest that monoamines may play a crucial role in auditory processing and that changes in both dopamine and norepinephrine neurotransmissions are associated with noise induced hearing loss. D2 receptor functionality was examined as a possible mediator of the noise-induced changes in the dopamine neurotransmission, but revealed no significantly alteration following noise exposure. Nonetheless, immunocytochemistry data demonstrated noise-induced attenuation in the receptor distribution in the inferior colliculus, an effect that implicate the D2 receptors in deafness related changes in the inferior colliculus. Overall, the combination of FSCV and immunocytochemistry provided new insights and sets the stage to further understand the role of monoamines in the central auditory processes.

TABLE OF CONTENTS

CHAPTER

LIST OF FIGURES

ACKNOWLEDGEMENTS

Several people have been essential in my success in achieving the completion of this thesis and my degree, and I am deeply grateful to all of them. I would first like to thank Dr. Aaron Apawu for being so supportive over the course of this research. It is amazing to see the lab transform from an empty space into something vibrant and functioning, especially with all the challenges faced when setting up and troubleshooting the instrumentation in the lab. Your excitement for science and your positive attitude has carried me through even the most frustrating periods. I am truly honored to be among your first graduate students. Next, I would like to thank my committee for their patience and insight in the development of my project. To my fellow graduate students, thank you for sharing in the stress and hardships of graduate life and I look forward to sharing a beverage with you all in the post-pandemic world. I'd also like to extend a special thank you to Kris, we've shared this journey together, in class or while battling troublesome instruments in the research lab. Your friendship and sense of humor has been invaluable to me. I would also like to acknowledge Aaron Updike, as an undergraduate in our research group, your help with data processing has saved me hours of time. To the UNCO Department of Chemistry and Biochemistry, for funding my graduate studies. Finally, I would like to thank my wife, Lindsay. Your love and support have guided us from the East coast in Virginia all the way back to our home in Colorado. I would not be where I am without your loving devotion.

CHAPTER 1

INTRODUCTION

Hearing-related disorders are prevalent all over the world and can be caused by exposure to loud noise encountered through recreation, or occupation. In the United States, the effects of hearing loss impact approximately 48.1 million people (F. R. Lin et al., 2011). Evaluations by the Centers for Disease Control and Prevention (CDC) indicate nearly a quarter (24%) of working adults have a proclivity for noise-induced hearing loss (Carroll, 2017). Of these working adults, approximately 30 million are exposed to hazardous levels of noise with another 9 million exposed to ototoxic chemicals (Yankaskas, 2013). Veterans stand apart as a uniquely impacted group, according to the Department of Veteran's Affairs, with tinnitus and hearing loss being the top two disability claims. These two disabilities result in $1.8 billion in estimated compensation (Huddle et al., 2017). Tinnitus differs from hearing loss and is described as the development of acoustic phantoms, which are characterized as persistent ringing and/or buzzing sounds in the ear. Currently, there are no objective measures for how tinnitus is measured or diagnosed aside from qualitative means. Furthermore, the extent of damage that noise can impart upon the brain is not well understood.

A number of studies have reported the effects of noise on the central auditory system, with most of these studies suggesting that exposures to loud noise trigger spontaneous neuronal activity in auditory brain regions (Chen et al., 2016; Basta & Ernest, 2004; J. S. Zhang & Kaltenbach, 1998). Further growing evidence suggests a connection between the peripheral effects of noise damage with central consequences in the nervous system. A comparative study

between tinnitus and non-tinnitus patients utilizing functional magnetic resonance imaging (fMRI) demonstrates increased activation of the inferior colliculus by sound stimulation (Middleton & Tzounopoulos, 2012). This effect has also been exemplified by a similar study using Magnetic Resonance Imaging (MRI), which indicated a reduction in glucose metabolism within areas of the auditory cortex and inferior colliculus from individuals suffering from hearing loss (Speck et al., 2020). Furthermore, patients with central nervous system pathology, like Parkinson's disease, associated with depletion of dopamine, exhibit a proclivity towards deficits in their auditory processing (Folmer et al., 2017; Lai et al., 2014). This observation implicates monoamines, like dopamine, in auditory processing.

Dopamine is a neurotransmitter well-known for its role in learning, memory, cognition, voluntary movement, and reward-related behaviors, but is not typically associated with hearing. Currently, however, significant amounts of data exist that suggest dopamine's role in hearing. For instance, changes in tyrosine hydroxylase (TH), the rate-limiting enzyme in dopamine synthesis, and dopamine receptor gene expressions have been reported in the dorsal cortex and the central nucleus of the inferior colliculus, and also within the intermediate lemniscus following deafness (Tong et al., 2005). A follow-up study also indicates these changes persist in the cochlear nucleus and inferior colliculus following acoustic trauma (Fyk-Kolodziej et al., 2015). Electrophysiological experiments have shown dopamine within the inferior colliculus affects auditory responses in a heterogeneous manner (Gittelman et al., 2013a). Despite the presence of this evidence, the way dopamine neurotransmission modulates auditory processes, particularly within the inferior colliculus, is still not well understood.

The present work was designed to bridge this gap by first, optimizing an electroanalytical method, fast scan cyclic voltammetry (FSCV) to detect, characterize, and quantify monoamine

release and uptake within the inferior colliculus. The inferior colliculus is an important brain region in the central auditory pathway, as it integrates auditory inputs from both ascending and descending pathways. Tract tracing and electrochemical studies have demonstrated that dopaminergic neurons in the subparafasicular thalamic nucleus (SPF), a non-auditory region, innervate the inferior colliculus (Batton, et al., 2019; Nevue, et al., 2016). This suggests non-audiologic neurons have a connection and role in auditory processing.

Second, the effects of loud noise on monoamine neurotransmission were characterized and compared. This objective was achieved utilizing FSCV with pharmacological manipulations. Previous comparisons between deaf and normal subjects have displayed a marked-down expression for both enkephalin, an opioid receptor, and tyrosine hydroxylase (TH), respectively (Holt et al., 2005a). This suggests a lack of expression of dopamine synthesis from TH would result in an overall downstream decrease in affected dopamine neurons.

Third, the mechanism behind monoamine activity within the inferior colliculus was explored by examining dopamine receptor functionality. Dopamine receptors are categorized into D1-like and D2-like receptors. The D1-like receptors are involved in excitatory functions, whereas the D2-like receptors are inhibitory in their action. Characterizing these receptors in the inferior colliculus will provide information about the type of dopaminergic transmission that predominates the region. This objective was achieved through the combination of FSCV with pharmacology and immunoassays, such as immunocytochemistry.

Altogether, this proposed work laid the necessary foundations towards understanding the role of monoamines in hearing. Furthermore, insight garnered from this work may contribute to both a route for therapeutic innovations, and the development of objective measures towards characterizing noise-induced hearing disorders.

1.1 Specific Research Objectives

Although substantial research data exist to implicate dopamine in processes both in the peripheral and central auditory pathway, the specific neural action of the neurotransmitter is not known. The presented work focused on the inferior colliculus to begin to define the neural action of dopamine neurotransmission in the central auditory pathway. The inferior colliculus acts as the integration center for both ascending and descending neural auditory pathways. The region also receives innervations from non-auditory neural sources. Herein, dopamine's neural action in the inferior colliculus was explored under three main objectives.

O1   Optimization of a FSCV assay to characterize dopamine neurotransmission in the inferior colliculus.

The inferior colliculus has been extensively studied using techniques, such as sound-evoked responses (Shaheen & Liberman, 2018), frequency-followed responses (Wang & Li, 2018), and electrophysiology (Gittelman et al., 2013a). However, the role of dopamine neurotransmission in the inferior colliculus has not been characterized. Recently, retrograde tracing has been used to identify the subparafasciular thalamic nucleus (SPF) as a source of dopamine in the inferior colliculus. In that experiment, the SPF was found to be the only nucleus where the retrograde label was detected in connection with the inferior colliculus, hence establishing the SPF as the primary source of dopamine to the inferior colliculus (Nevue et al., 2016). The present work was built on this foundation by characterizing the dopamine neurotransmission in the inferior colliculus using slice fast scan cyclic voltammetry (FSCV). Herein, the FSCV technique was optimized by characterizing the figures of merit for dopamine detection and differentiating the sensitivity from interfering analytes.

O2   Characterizing the effects of loud noise on monoamine neurotransmission in the inferior colliculus.

Existing data has demonstrated change in tyrosine hydroxylase gene expression is significantly reduced following acoustic trauma (Fyk-Kolodziej et al., 2015; Holt et al., 2005b; Tong et al., 2005). These changes suggest that dopamine is involved in deafness- related plasticity in the inferior colliculus. Based upon this data, we hypothesize that loud noise could alter the dopamine neurotransmission in the inferior colliculus. The present objective thus, examines the effects of noise on the dopamine release and uptake, as well as the functionality of dopamine receptors. Comparative FSCV experiments was be performed between control and sound exposed subjects to indicate the effects on dopamine neurotransmission. This work provided insight about the neuronal basis of noise induced hearing deficit and could pave way for future interventions and therapies.

O3   Exploring a plausible mechanism underlying the deafness- related changes in monoamine neurotransmission.

Dopamine's activity can be functionally described by which types of receptors are present. Two primary receptor families are associated with dopamine transmission, namely D1-like and D2-like receptors (Jaber et al., 1996). Five subclassifications further characterize these receptors according to their more specific neurological function. While dopamine receptor gene expression has been reported in the inferior colliculus (Fyk-Kolodziej et al., 2015), neither the levels, nor the functionality of these receptors has been shown. Under this objective, both the levels and the functionality of D1 excitatory and D2 inhibitory receptors were characterized, and we sought to understand whether the dopaminergic inputs in the inferior colliculus are excitatory or inhibitory in their function. This also provided insight as to the role dopamine may play in the inferior colliculus.

CHAPTER 2

LITERATURE REVIEW

2.1 Sound Processing Through the Auditory
Nervous System

The path of sound through the auditory system is essentially similar across all mammals. Soundwaves are collected by the pinna, much like a funnel. Here, the waves are transmitted through the auditory canal until reaching the eardrum, or tympanic membrane. The sound wave vibrates the tympanic membrane, causing the movement of a series of bones within the middle ear. These bones are the malleus, incus, and stapes (Figure 1). The vibration of these bones subsequently moves a vast multitude of tiny hair cells in a snail-shaped structure called the cochlea. Through electro-mechanical transduction, the hair cells transform the vibrational patterns of sound into neural signals. The stretching sensation of the hairs triggers ion channels resulting in the creation of an action potential, the electrical impulse which transmits neural messages. The passage of signal from the cochlear hair cells into the vestibulocochlear nerve (cranial nerve VIII) marks the transition from the peripheral to the central auditory pathway.
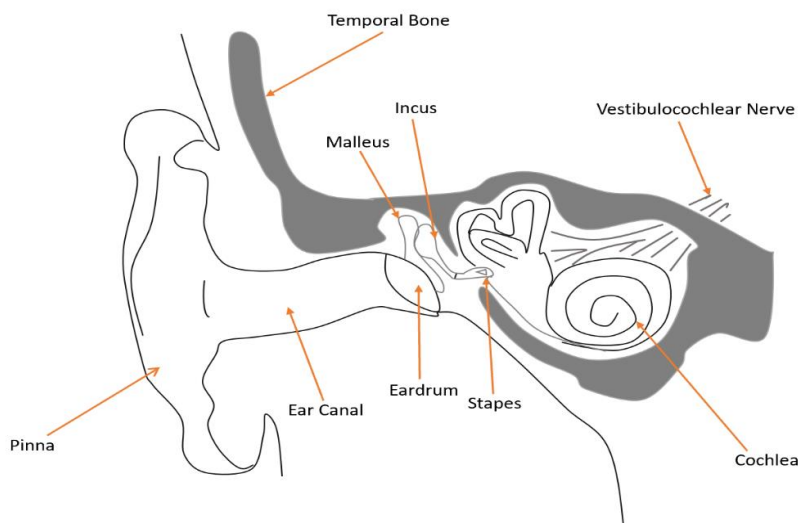
Figure 1. A cross sectional view of the peripheral auditory anatomy.

Input from the vestibulocochlear nerve ascends through a series of neural nuclei until reaching the auditory cortex, where the sound is ultimately perceived (Figure 2). The connection with the auditory cortex is achieved through several neural relays. First, the message is received at the cochlear nuclei within the brainstem. Most of the signal decoding happens here, which is responsible for discerning the frequency, duration, and intensity of the soundwave. Next, continuing further within the brainstem, is the superior olivary complex. Sound localization begins here, where the majority of the auditory nerves cross the brainstem's midline. Third, the lateral lemniscus contains the connections from the contralateral cochlear nuclei, with the ipsilateral superior olivary complex forming a single tract. These fibers ascend further, converging at the inferior colliculus (Cope et al., 2015). At the inferior colliculus, both the ascending and descending auditory pathways are conserved. Due to the extensive integration of auditory and non-auditory neural inputs, the inferior colliculus is commonly referred to as the call center of the central auditory system. The last relay before entering the auditory cortex is the medial geniculate body, which is responsible for the integration of the sound information in preparation for other actions (Peterson & Hamel, 2019). Ending at the auditory cortex, the neural

signal has been decoded, recognized, and can be further memorized and/or integrated into a response.

Auditory Cortex

Medial geniculate nucleus

Inferior colliculus

Dorsal cochlear nucleus

Ventral cochlear nucleus

Incus

Stapes

Malleus

Ear drum

Cochlea

Superior olivary complex
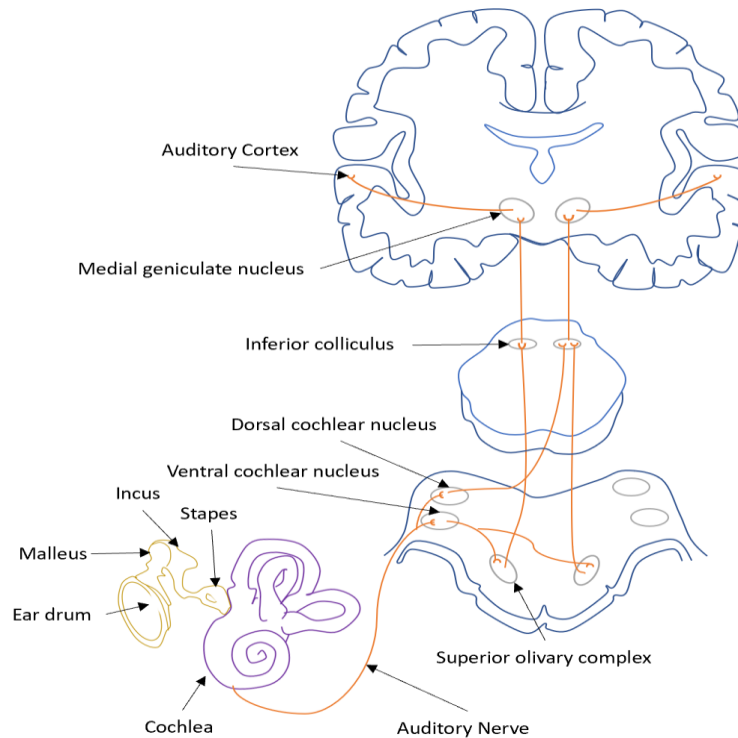
Auditory Nerve

Figure 2. Overview of the central auditory system. Neural innervations entering the brain from the cochlea. Auditory inputs integrated at the inferior colliculus.

2.2 Neurotransmission and Neurochemicals

The functional activity within the nervous system operates through the reception of stimulating input and the means by which these signals are processed. Propagation of these neural messages through the nervous system defines neurotransmission. Following the delivery of a stimulus, neurons conduct these signals through an electrochemical gradient called an action potential. These electrical potentials are achieved through the multitude of ion channels and pumps located along the neuron, which create a charge disparity between the nerve terminal and the extracellular space. These ions produce a gradient of charge that creates the environment,

providing the electric pulse to move down the nerve terminal quickly and efficiently, much like the flow of electrons through a wire.

Unlike wires, which exist as one continuous connector to another, nerve terminals are separated by a small gap between the clefts of the neural cells, called the synapse or synaptic cleft. The intricacies of these neural protein receptors at this junction is where the nuance of the nervous system is expressed. These neurons contain myriad neurochemicals which are released to propagate a specific signal in response to the invoked stimulus. Categorized as neurotransmitters, these molecules are chiefly responsible for the diversity of operations carried out by the nervous system. Following the synthesis of these neurochemicals, they are packaged within vesicles waiting for the activity of an action potential to foster their release.

Dopamine is a neurotransmitter widely known for its role in learning, memory, cognition, and reward-related behaviors. The pathway of dopamine synthesis classically begins with conversion of L-phenylalanine into L-tyrosine. Enzymatic hydroxylation catalyzed by tyrosine hydroxylase (TH) produces L-3,4-dihydroxyphenylalanine (L-DOPA), a catechol moiety. Decarboxylation of L-DOPA from aromatic amino acid decarboxylase (AADC) yields dopamine (Figure 3). Next, dopamine is either packaged into vesicles for later use or shuttled further down the catecholamine synthetic pathway and converted into norepinephrine.
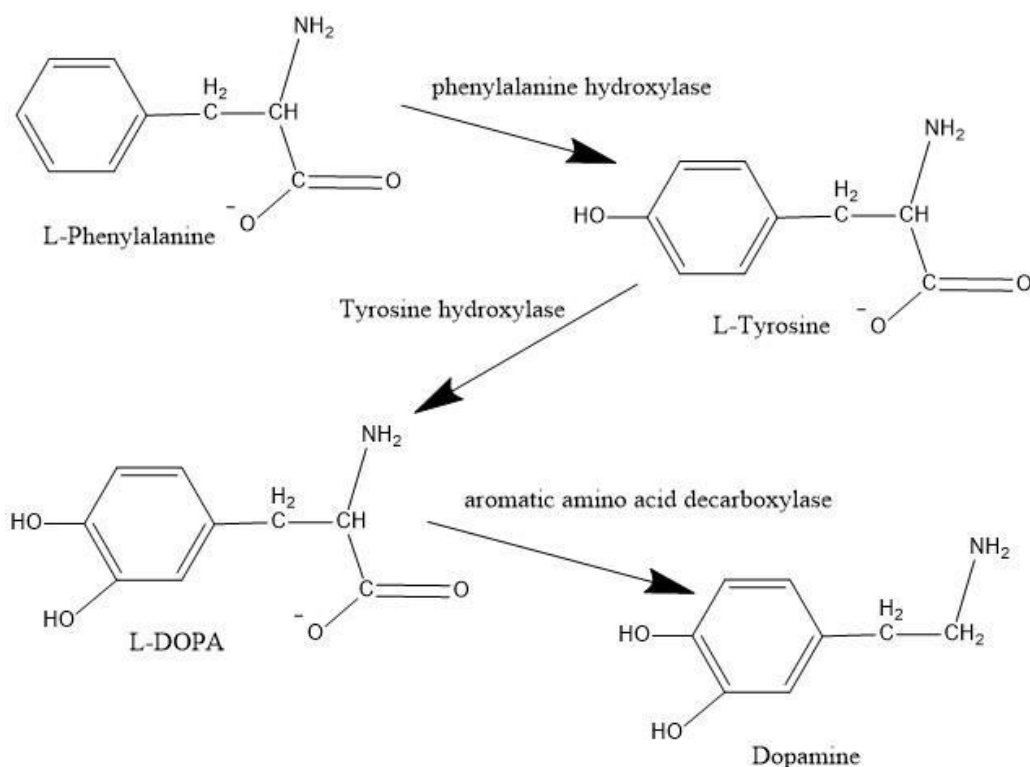
Figure 3. Summary of dopamine synthesis occurring within the cytosol of neural cell bodies.

As the electrical impulse passes down the nerve fiber, it eventually reaches an endpoint along the axon terminal where the neurochemically loaded vesicles are signaled to fuse with the cell's outer membrane, releasing their contents into the synaptic cleft (Figure 4). These released neurochemicals then seek to bind to specific receptors on the receiving nerve terminal to further propagate the neural message. Previously bound, as well as unbound and excess, neurotransmitters are either recycled back into their sending neuron or degraded into metabolites within the synaptic space.

Dopamine is broken down through a series of enzymatic reactions. The order of this process is sometimes variable, due to the complex nature of dopamine neurotransmission. Either through monoamine oxidase, catechol-O-methyl transferase, or aldehyde dehydrogenase, the final metabolic end product is homovanillic acid (Figure 5).
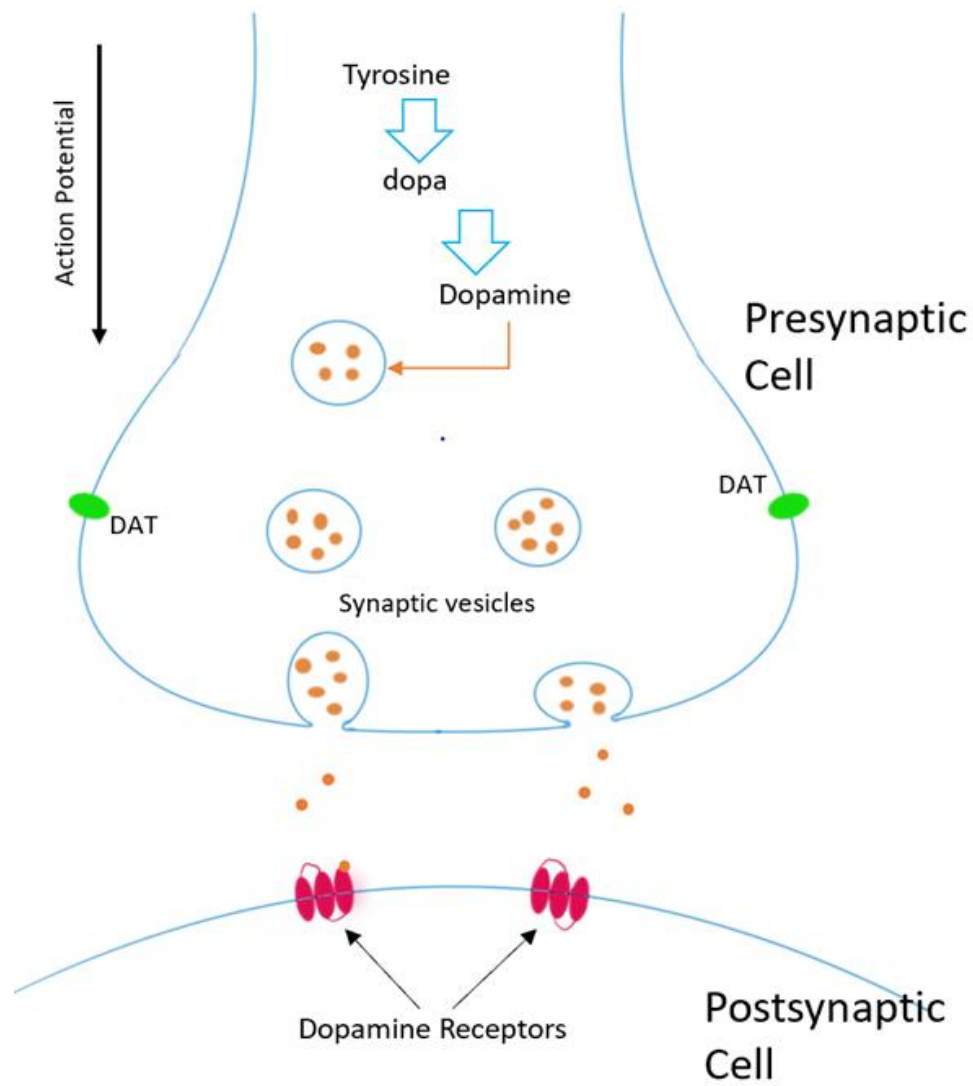
Figure 4. Generalized diagram of dopamine neurotransmission. Action potentials facilitate neurotransmitter release into the synaptic space where neurochemicals interact with target receptors. Binding further propagates physiological responses, such as learning, reward, motion, etc. Unused chemicals are either recycled or metabolized.
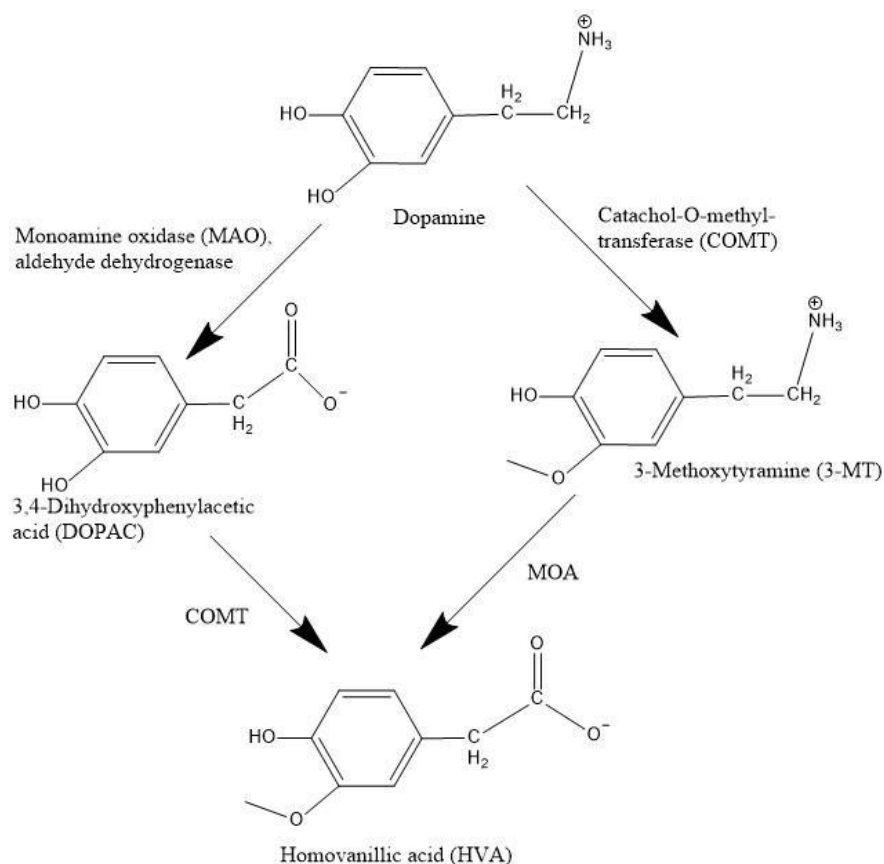
Figure 5. Summary of dopamine metabolism. The order of each enzymatic process is not exclusive to a singular pathway and may involve a different order.

Dopamine-based receptors are organized into two distinct families (D1-like and D2-like) (Jaber et al., 1996). D1-like receptors are multi-functionally associated with the reward pathway-learning, locomotion, and memory. These receptors are excitatory and enhance neuronal activity. In contrast, the D2-like receptors are inhibitory in nature, suppressing neuronal excitability and inhibiting dopamine release. Receptor distribution within the brain region of interest can help shed light on which neurological function, inhibitory or excitatory, predominates.

2.3 Tools for Brain Measurements

For a technique to be suitable for neurochemical measurements, it must have high spatial resolution, speed, sensitivity, and selectivity (Lama et al., 2012). Nerve terminals have already been established to be small, and the amounts of neurochemicals transferred are as equally

minute. Low concentrations of neurochemicals necessitate the selection of an instrumental method capable of detecting the analyte, while also being able to discriminate against the background signal. The most commonly used techniques for neurochemical measurements include imaging, sampling, and separation tools, such as microdialysis coupled to chromatography, and electroanalytical techniques.

Imaging methods extend throughout a broad application in both research and medicine. Visualization of neural environments can span the entire brain, using tools such as MRI (Ferraro et al., 2014), positron emission tomography (PET) scans (Tuominen et al., 2014), or radioactivity. Utilization of contrast agents, such as fluorescent probes (M. Z. Lin & Schnitzer, 2016) or nanoparticles (Moussaron et al., 2015), become necessary to properly view the neural dynamics of the system. Many of these methods provide non-invasive means for testing neural environments in vivo.

Though the field of imaging continues to improve and evolve, the implementation in neuroscience research faces many challenges. Primarily, the cost of such detection systems becomes inhibitory in and of itself, with many of the instruments ranging from hundreds of thousands of dollars. The usage of complex and expensive contrast and detection agents only limit the usage of these imaging techniques in neuroscience research. The intricacy of both the instrumentation and the subjects of study also further the difficulties of these techniques in more common practice.

Sampling and separating methods provide the unique capabilities of monitoring and detecting analytes simultaneously. Most of these techniques seek to quantify neurochemicals, and their associated substituents, extracellularly. Common examples include microdialysis (Gu et al., 2015; H. Yang et al., 2013) and high-performance liquid chromatography (HPLC) (Schou-

Pedersen et al., 2016). These methods effectively maintain specimen viability while allowing incorporation of different detection capabilities. The diversity of the instrumental components provides an approach to adaptability of the analytical tool in the face of separating out the bulk tissue components. Separation methods operate most efficiently when the samples are previously extracted for analysis.

Compared with the other categories, imaging and electrochemistry, sampling/separation methods are limited in temporal resolution. Large probes used in microdialysis also create issues in spatial resolution. The tissue becomes disrupted creating peripheral damage and inviting host immune responses. Reproducibility is also restricted with these methods, as much of the initial sample can become degraded or destroyed during the data acquisition process. However, the vast array of options available under these techniques will continue to provide an essential tool in analytical analysis.

Electrochemical detection of neurochemicals was first characterized in the 1980s. Since then, techniques such as amperometry and voltammetry have provided expansive information of electroactive chemicals involved in neurotransmission, chiefly through alterations in analyte redox potentials along the varying electrode surfaces. This early work has become the foundation of several present clinical and research instrumentations (Webster, 2009). These methods mainly seek the analysis of neurotransmitters through either cellular exocytosis, *in vitro* or *in vivo* experimentation. The highly sensitive and temporal resolution of these techniques make them ideal for neuroscience research.

Exocytosis techniques, including amperometry, are most useful when studying neurotransmitter release (Lemaître et al., 2014). Comparison of chemical release across differing cell types is where these types of instruments excel. The quantity of neurochemicals released

does not convey the total amount present in the neuron, as most of the content of neurochemicals within their vesicles is retained. The inability to gauge the number of secretory neurochemicals remains a consistent critique of these techniques. Enhancement of microfluidics has yielded promise in expanding such techniques beyond neurochemical research.

In vitro and *in vivo* studies are the most attractive applications of electrochemistry in neuroscience research. The combination of spatial resolution, limits of detection, and speed place electrochemical analysis apart from much of the other categories (Lama et al., 2012). Additionally, the cost and maintenance of electrochemistry instrumentation is a fraction of what it costs to purchase and maintain imaging equipment.

2.3.1 Fast Scan Cyclic Voltammetry

Fast scan cyclic voltammetry (FSCV) stands out as both a historic and modern methodology for neurochemical measurements. When coupled with a carbon fiber microelectrode, FSCV exhibits the high spatial resolution, speed, sensitivity, and selectivity required for neurochemical measurements (Lama et al., 2012). Like classical cyclic voltammetry, the FSCV technique involves an application of a potential at an electrode surface in the form of a triangular wave. In FSCV, however, the potential is applied at a high scan rate. Rapid measurements can be recorded under these high scan rates over the course of milliseconds, allowing for high temporal resolution. Repeats of these waveforms deliver kinetic information regarding the concentration of these electroactive species (Roberts & Sombers, 2018). However, the current produced solely from the electrode is typically greater than the physiological presence of the neurochemicals. To overcome this challenge, background subtraction is used to measure the changes of a FSCV signal from a reference point (Rodeberg et al., 2017).

FSCV has been widely used to study the dopamine system. Dopamine, like other monoamine neurotransmitters in the brain, is electroactive. Following the forward scan of the applied potential, typically from -0.4V to 1.3V, dopamine is oxidized to form dopamine-o-quinone, whereas in the reverse scan dopamine-*o*-quinone is reduced back to dopamine (Figure 6). The flow of electrical charge involved in the redox reaction is measured as current, which is proportional to the concentration of the analyte, according to Faraday's law of electrolysis.
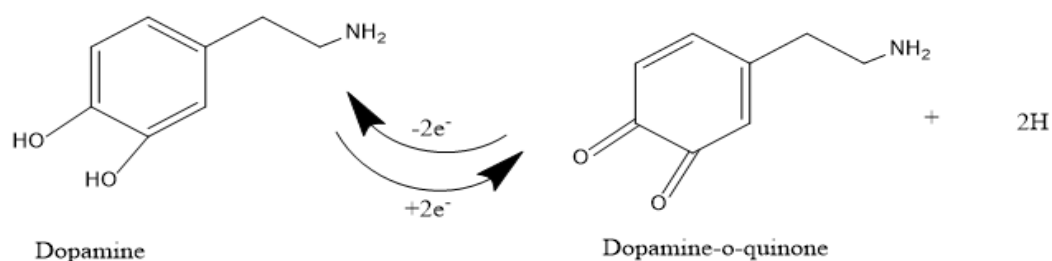
Figure 6. Redox reaction of dopamine. Dopamine oxidizes to dopamine-o-quinone at a characteristic electrode potential, whereas dopamine-o-quinone reduces back to dopamine at a suitable reduction potential.

Data collection in FSCV can be represented in three different forms: a cyclic voltammogram, a current versus time plot, and a pseudo-color plot (Figure 7). Voltammograms are obtained from the change in potential through the rapid application of waveforms. The redox activity of the analyte acts as the signature to selectively identify the analyte of interest. Time plots are the product of Michaelis-Menten kinetics equations. The pseudo-color plot marks the incorporation of the previous two plots. Current stands out as the colored component representative of the z-axis of the plot, with time and the applied electrode voltage designated as x and y-axis, respectively.
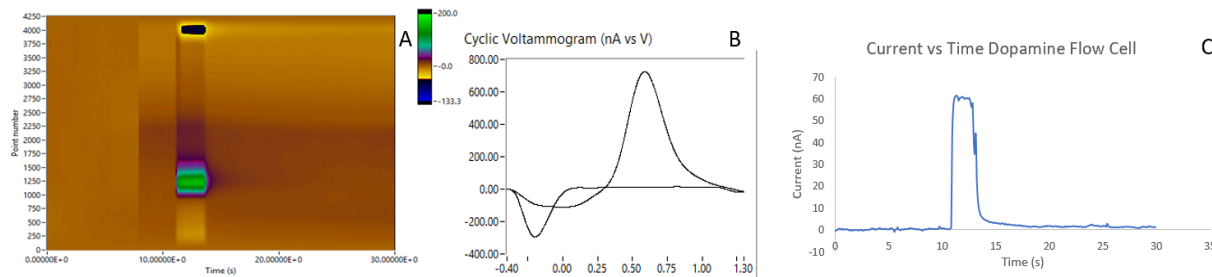
Figure 7. Types of data collected from FSCV measurements. (A) Pseudo-color plot displaying the applied potential over time; green indicates oxidation, black/blue denotes reduction. (B) cyclic voltammogram characterizing the specific redox of dopamine: oxidation peak at approximately +0.6 V and the reduction peak at -0.3 V. (C) Current vs time plot, indicating the redox activity at the electrode surface. Currents can later be converted into concentration terms via Faraday's Law.

2.3.2 Advantages of Fast Scan Cyclic Voltammetry

The high temporal resolution of FSCV further separates it from other analytical techniques used in neurochemical measurements. FSCV also exhibits the capability of a fast sampling rate, covering a milliseconds range (Lama et al., 2012). This action is achieved through the delivery of a negative waveform potential, yielding an increase in the hold of dopamine concentrations. By promoting this holding potential, more absorption can occur along the carbon fiber electrode, providing a greater selectivity when compared to alternative analytical methods. *In vivo* studies are another realm appealing to the utilization of FSCV (Figure 8). Through the implantation of electrodes in animal subjects, voltametric recordings can be made in real-time. The ability to collect data within the native environment of a subject yields valuable evidence regarding the mechanisms involved in neurotransmitter release and uptake events (Robinson et al., 2003).

Figure 8. Stereotaxis apparatus example. (A) Arms contain measurement knobs (in mm) which direct probe placement into the subject. (B) Nose bar which fits over the mouth and nose to secure the subject and orient head tilt. (C) Ear bars also secure the subject and orient measurements for electrode implantation. (D) Alternate view of stereotaxis arm, which can hold electrodes for subject implantation.

The space within the synapse is small, between 10 to 100 nm. Carbon fiber has emerged as the material of choice due to its small size, ease of electrode fabrication, and relatively inert chemical properties (Figure 9). The use of carbon fiber electrodes allows for measurements within the micrometer range and is associated with minimal tissue damage (Abdalla et al., 2017).
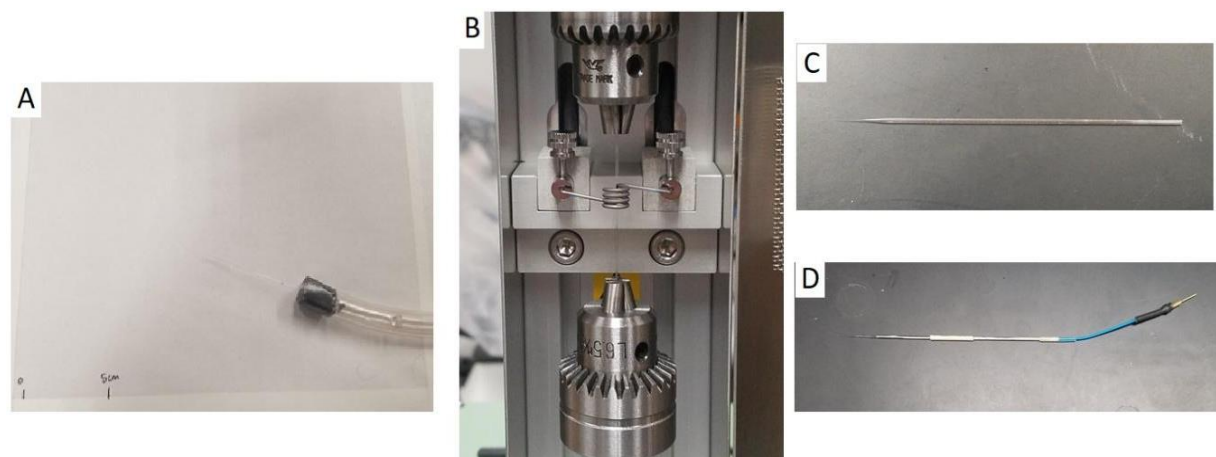
Figure 9. Electrode fabrication process. (A) Carbon fiber is aspirated through borosilicated glass using vacuum suction. (B) Glass capillaries are pulled by heating and melting the glass to form a seal with the carbon fiber. (C) The pulled electrode is inspected for quality of the fiber and cut to between 50 and 100 microns under a microscope. (D) The electrode is connected with a wire and pin, reinforced with heat-shrink, and can now be connected to the potentiostat.

FSCV can also be used with brain slices (Figure 10), with the primary advantage being the ability to provide presynaptic control over dopamine release. The technique also limits the effects from dopaminergic cell bodies through artificial stimulation by using a stim electrode, which allows for the focus to be on the presynaptic dynamics (Maina et al., 2012). The addition of pharmacological agents is also more convenient under slice FSCV. Under *in vivo* conditions, applied agents require sufficient clearance time between recording measurements.
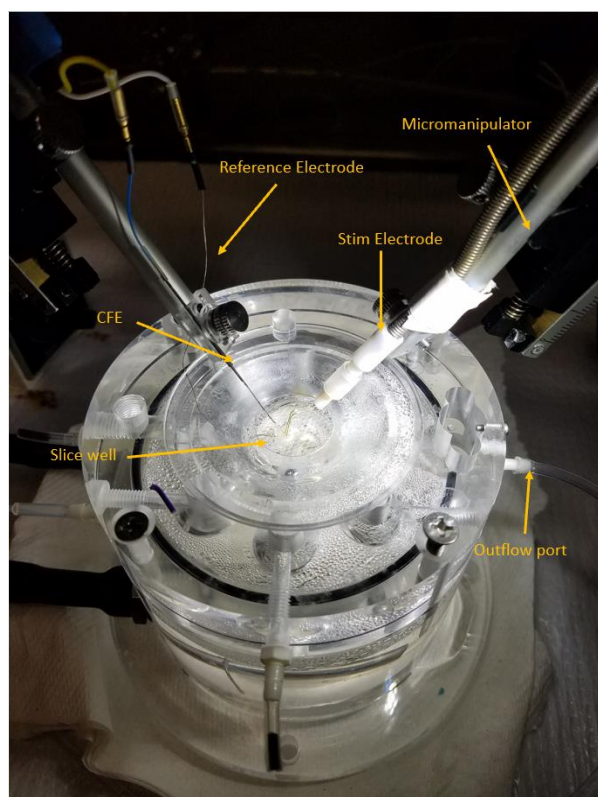
Figure 10. Example of *in vitro* FSCV set-up where brain slices are stimulated within the slice well. Electrodes are positioned with micromanipulators and the tissue is constantly perfused with oxygenated artificial cerebrospinal fluid (aCSF).

Slice FSCV is ultimately limited by the effects of dissection of the tissue sample. Due to the separation of large sections of the tissue most of the complex connections of the neural pathway have been severed. Connections and innervations from different brain regions are made inaccessible under these experimental conditions, keeping the utility narrow.

2.3.3 Innovations in Fast Scan Cyclic Voltammetry

Electrode modifications is one area of improving and innovating the performance of FSCV. Changes to the carbon fiber enhances the redox activity, allowing for a more extensive detection capability. Carbon fiber electrodes can be improved with nanotube modifications (C. Yang et al., 2016), or through coating the surface, such as treating the surface with 4-sulfobenzene (Hermans et al., 2006).

Paired pulse voltammetry (PPV) further advances the detection capabilities of FSCV through the addition of a secondary waveform. Instead of managing singular waveforms, paired pulse voltammetry deals with the procurement of binary (primary and secondary) waveforms; processed with a timed gap between each wave form. Both waveforms are collected according to their applied potential, just as in standard FSCV (Oh et al., 2015). Analytes and metabolites are differentiated according to their respective scan repetition time, sweep rate, and peak voltage of the triangular waveform (Jang et al., 2012).

Alternatively, neurochemical release can also be stimulated through light instead of electrical potentials. Optogenetics induces neurotransmission by incorporating photosensitive proteins into the host nerve of interest by genetic engineering. Light activation provides the advantage of increasing selectivity to only the neurons expressing the opsin proteins (Guru et al., 2015). Optogenetics, however, exhibits analogous information to electrically stimulated FSCV. Additionally, the instrumentation costs of optogenetics are exorbitantly more expensive when compared with the more cost effective conventional FSCV.

2.3.4 Immunoassays

Immunoassays like Western Blot and flow cytometry are also useful in detecting and measuring specific receptor proteins. Western Blot is a common technique used in the isolation and quantification of proteins. Homogenized tissue samples can have their proteins segregated by mass and charge through the utilization of size proportioned gel and electrophoresis (Taylor & Posch, 2014). Proteins appear in the gel as bands according to their exclusionary separation. The identity of the proteins is revealed by the specialized targeting with antibody-antigen staining. Concentration is measured through the strength in absorbance presented in the sample.

Dopamine receptors have previously been identified and quantified using Western Blot analysis (Levey et al., 1993).

A multitude of different proteins can be contained within each of the blot's bands. However, the combination of protein separation and immunoblotting act as the key advantages of this method. The expression of the tagged immunostaining complex maintains the specificity to identify the protein of interest. Western Blot also carries a low-cost instrumentation with an ease of repeatability for comparative analysis, which is attributed to the technique's enduring laboratory usage.

Immunocytochemistry offers a complimentary approach to protein analysis through the examination of the tissue's structural environment. This methodology integrates the specific protein areas via targeted antibodies in order to identify the precise analyte of interest and imaged using fluorescent or confocal microscopy (Mize et al., 1988; Nabors et al., 1988). Effects on protein receptors can be directly visualized and their localization as well as distribution can be compared to view the changes inflicted by the experimental parameters.

CHAPTER 3

MATERIALS AND METHODS

The methods described here encompass the use of biochemical assays and neurochemical techniques to characterize auditory brain function. All the experimental protocols involving animals used in this research were approved by the Institutional Animal Care and Use Committee (IACUC) of the University of Northern Colorado.

3.1 Chemicals

The reagents used to prepare the artificial cerebrospinal fluid (aCSF) for slice voltammetry were purchased from Fisher Scientific Co. (Fairelawn, NJ) and Sigma Aldrich (St. Louis, MO). Antibodies were procured from Alomone Laboratories (Jerusalem, Israel).

3.2 Animal Subjects

Thirty-two adult Sprague Dawley rats were used in this research project. This rat strain has been used extensively in previous work regarding the inferior colliculus. In rats, the inferior colliculus is larger and more easily characterized.

3.3 Noise Exposure Chamber

The noise chamber used in this work was fabricated in-house with the following dimensions: 36" wide x 30" long x 25.5" tall (Figure 11A). The interior of the chamber was lined with sound dampening foam to reduce the influence of the surrounding environmental noise (Figure 11B). Speakers are placed in an even square arrangement at 16" at each corner. The interior was lined with sound absorbing foam. In the ceiling of the chamber, four TW44 speakers

(Parts Express, Springboro, OH) were embedded in an evenly spaced manner and wired

according to a combined series/parallel schematic (Figure 11 C).
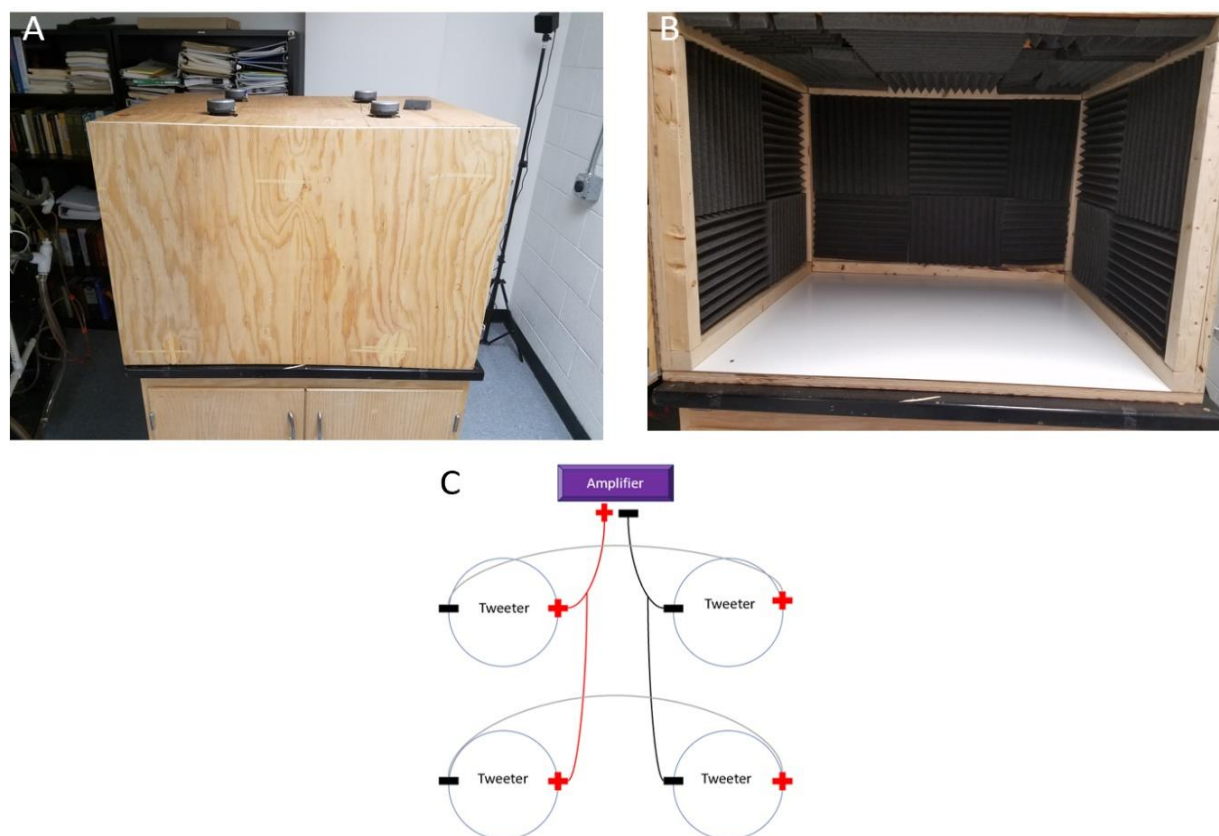
Figure 11. Noise exposure chamber. (A) Exterior of the chamber. (B) Interior of the chamber lined with sound dampening foam. (C) Schematic of series/parallel wiring arrangement of the sound exposure booth's tweeters providing a total impedance of 4 ohms.

The speakers are connected to a multicomponent sound amplification system as follows;

a Beringer NX-4000 amplifier (Parts Express, Springboro, OH), and a computer system to

control and deliver the appropriate tones/frequencies. The speakers to the amp were connected

via crimp terminals, alligator clips, and Speak-On respectively. The computer interface was

connected with the amplifier according to a 1/4" to standard audio jack which can be plugged

into the amplifier and computer, respectively. Sound delivered into the system was controlled

using Daqarta v10.5.2 software (Interstellar Research, Ann Arbor, MI). Noise exposures were set to 10 kHz at 118 dB sound pressure level (SPL) at 1/3 octave band.

3.3.1 Calibration of Noise Exposure Chamber

The sound chamber was calibrated by determining the average distance between the ceiling mounted speakers and the animal subject's ears. A Radio Shack digital sound meter (Fort Worth, TX) was used to measure the distribution of the sound cone from the speakers within three dB. The meter was also adjusted at a variety of different angles analogous to the location of the animal subject's ears and positions to ensure the appropriate sound (3 dB) overlap and evaluated any contributions in the sound box to random noise.

3.4 Fast Scan Cyclic Voltammetry System

3.4.1 Electrode Fabrication

Carbon fiber microelectrodes were made using the following steps. First, the carbon fiber (Goodfellow, Huntingdon, England) was separated into single strands and aspirated through a borosilicated glass capillary tube (A-M Systems, Sequim, WA) via vacuum suction. The capillary tube was then pulled using a Narishige PE-22 puller (Tokyo, Japan). This process sealed the glass capillary-carbon fiber interface. The exposed carbon fiber was then cut to an appropriate length using a microscope (Olympus, Center Valley, PA), according to a microscopic reticule between 50 to 100 μm. Next, the electrode was pinned and connected with a metal wire that had been coated with carbon paint (Alfa Aesar, Tewksbury, MA) to establish an electrical connection between the wire and the aspirated carbon fiber. Heat shrink was then applied at each end of the gap junctions where the connecting wire and glass capillary meet, as well as where the wire was soldered to the interface pin, to reduce noise and to reinforce the structural integrity of the microelectrode (Figure 12).
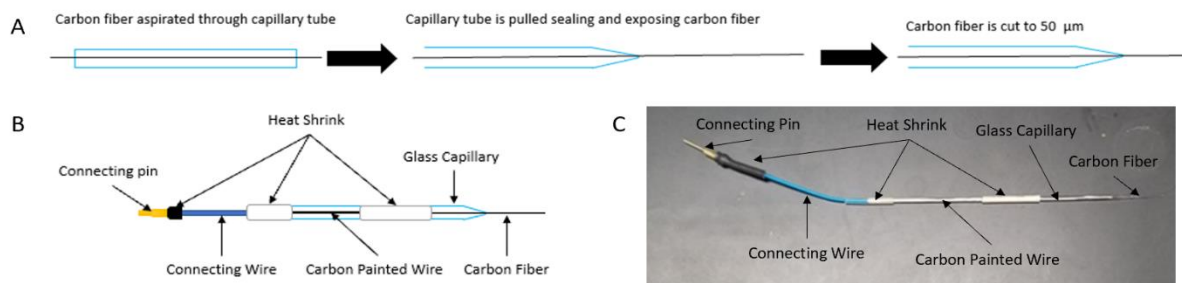
Figure 12. Progression of electrode fabrication. (A) Schematic of carbon fiber aspiration, pulling and cutting the fiber to an optimal length. (B) Schematic of completed carbon fiber microelectrode. (C) Example of completed carbon fiber microelectrode.

3.4.2 Electrode Conditioning and Calibration

The process of conditioning the electrode was achieved through the continuous cycling of the waveform on the electrode. A higher cycling frequency was used to etch the electrode surface thereby increasing the sensitivity to electroactive species under this potential window. This step, in turn, improves the electrode's capability towards the electroactive species at the applied waveform. A 60 Hz frequency was applied to achieve this conditioning for approximately 5 minutes, or until the oscilloscope signal was stabilized, where a smooth charge to discharge indicates a good electrode (Figure 13).
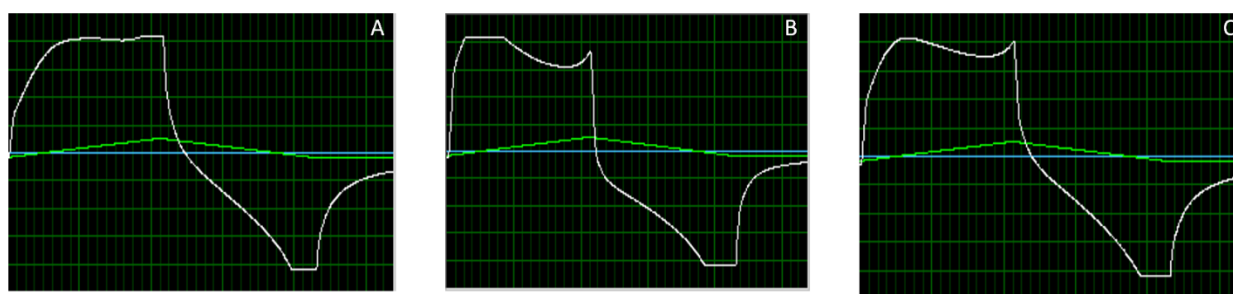
Figure 13. Oscilloscope of a CFME cycling at 60 Hz. (A) Initial electrode status is resistive due to the flattened peak. (B) Electrode displays the shifting discharge profile. (C) Electrode maintains a stable charge to discharge peak, indicative of a good electrode.

Next, the calibrated electrode was characterized by determining its sensitivity and effectiveness as well the reproducibility of the signals. A three port T-flow cell was used to make

these measurements. An Ag/AgCl reference electrode was sealed in the center of the cell. The

first of the side ports being used to introduce a continuously perfusing modified cerebrospinal

fluid via a syringe pump at a flow rate of approximately 2 mL/min. The calibration buffer was a

modified form of the artificial cerebrospinal fluid used in slice voltammetry. The buffer was

composed of 126 mM NaCl, 2.5 mM KCl, 2.4 mM $CaCl_2$, 1.2 mM MgCl, 1.2 mM Na_3PO_4, 25

mM $NaHCO_3$ set to a pH = 7.4, as described by (Maina et al., 2012). The second port was used

to manually inject about 0.5 to 1.0 mL of a prepared 500nM dopamine standard through a

syringe into the cell. The dopamine was detected at the electrode surface according to the change

in the peak current measured (Figure 14). This process was repeated several times in order to

obtain an average peak current related to the consistent concentration of the dopamine injected.

This procedure was performed before (pre-calibration) and after (post-calibration) data

acquisition from brain slices. The calibration factor was determined from the analysis of the

electrode responses.
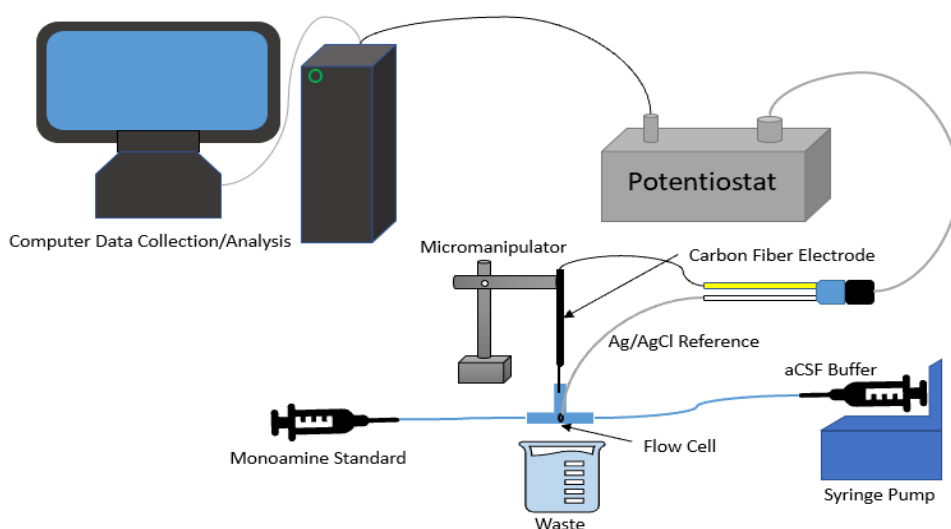
Figure 14. Schematic of the flow cell FSCV set-up for electrode calibration and characterization. Electrodes are characterized through the utilization and comparison between different

standards. Dopamine is recorded first as it is the analyte of interest. Next, ascorbic acid is

analyzed, as it is the chief interferant in biological measurements. The unique waveform signature generated acts as the primary differentiation between both standards. Ascorbic acid produces a single oxidation peak at approximately +0.8 V, where dopamine yields one oxidation peak at +0.6 V and one reduction peak at -0.25 V. The distinctive shape of each chemical supplies the details to gauge the performance of the selected electrode.

3.4.3 Slice Fast Scan Cyclic Voltammetry Data Collection

Prepared prior to the extraction of rat brain tissue, sucrose aCSF was prepared and used for vibratome sectioning of brain slices. Composition of the sucrose aCSF was 30 mM NaCl, 4.5 mM KCl, 1 mM $MgCl_2$ 26 mM $NaHCO_3$, 1.2 mM NaH_2PO_4, 10 mM D-glucose, 180 mM sucrose. The buffer was then oxygenated with carbogen gas (95% O_2/ 5% CO_2) for approximately 15 minutes before refrigerating it. The buffer was good for up to a week under these conditions. Animal subjects were sacrificed using an induction chamber (Harvard Apparatus, Holliston, MA) via CO_2 asphyxiation. Next, the brain was quickly removed and placed immediately into the chilled sucrose aCSF.

The extracted brain tissue was mounted with super glue onto a removable stage on a 1500 series vibratome (San Macros, CA). The cold sucrose aCSF was used to fill a tray surrounding the sample tissue to keep the brain viable throughout sectioning. Coronal slices were taken from the brain tissue at 400 micron thickness to fully encompass the region of interest (inferior colliculus). The slices were then transferred into the running buffer, where they were left to equilibrate in bubbling carbogen gas for one hour.

A brain slice was placed in an automate scientific slice chamber (Berkeley, CA) where a recording aCSF buffer composed of 126 mM NaCl, 2.5 mM KCl, 2.4 mM $CaCl_2$, 1.2 mM

MgCl$_2$, 25 mM NaHCO$_3$, 1.2 mM NaH$_2$PO$_4$, 11 mM D-glucose, 0.4 mM ascorbic acid; was being continuously perfused with carbogen at 2 mL/min by a Watson-Marlow peristaltic pump (Wilmington, MA). The recording chamber was also held at a 37°C temperature using a temperature controller (Automate Scientific, Berkley, CA).

Dopamine release was induced from the brain region of interest using electrical stimulation using a positive monophasic polarity with a frequency of 60, an amplitude of 4.5, and a pulse length of 4 ms. The electrical stimulation was generated by a Neurolog stimulation generator (Herfordshire, UK) and administered onto the brain slice through a stimulating electrode (Plastics One Inc, Roanoke, VA). Detection and characterization of dopamine release and uptake was achieved through the application of a triangular waveform potential at the carbon fiber working electrode surface. The electrical potentials span from -0.4 V to +1.3 V and back to -0.4 V at a scan rate of 400 Vs^{-1} every 100 ms with a frequency of 10 Hz, over a recording period of 10 seconds. An Ag/AgCl electrode was used as a reference electrode embedded in the recording chamber and connected to the white reference junction on the headstage. Once a stable signal was acquired, stimulations were then applied every 5 minutes to provide the neurons time to replenish the neurochemical stores within the synaptic cleft. Pharmacological manipulations of the brain slices were done using to determine or confirm the identity of the neurochemical present in the brain region. The main hardware components consisted of an integrated national instruments PCIe-6363 multifunction I/O device (Austin, TX) connected to a Pine Research Waveneuro potentiostat (Durham, NC). Data was generated by HDCV software (Chapel Hill, NC). A variety of computer software was incorporated to gather and analyze the data from this research. High Definition Cyclic Voltammetry (HDCV) software from the University of North Carolina (Chapel Hill, NC) and Wild Cat Cyclic Voltammetry software (WCCV)from Dr. Hein's

lab at the University of Arizona (Tucson, AZ) were used in coordination with the potentiostat systems to collect and analyze the electrochemical data. The entire system was shielded from electrical noise using a Faraday cage (Automate Scientific, Berkeley, CA).

3.4.4. Pharmacological Manipulations

Brain slices were treated with pharmacological agents to assist in identifying the source of the peaks observed during FSCV. Tetrabenazine (TBZ), a Vmat antagonist which reduces monoamine release, was prepared from a stock solution dissolved in ethanol before being further diluted. A 10 μM working dose was prepared from the stock solution and diluted in the aCSF running buffer. 50 μM αMPT, a tyrosine hydroxylase inhibitor, was prepared in a typical 0.9% saline solution.

Once the FSCV signal was stable, the running buffer solution was replaced with a buffer solution containing one, or a combination of, the previously mentioned pharmacological agents. Following perfusion, data collections were continued according to 5-minute stimulus intervals for 30 minutes per a drug concentration. The dosage was increased every 30 minutes until the last dose.

3.5 Immunocytochemistry

Changes in dopamine receptor protein localization and distributions in the inferior colliculus of the brain were characterized by immunocytochemistry (ICC).

3.5.1 Tissue Preparation and Staining

Control and sound exposed subjects were euthanized using carbon dioxide asphyxiation, the brain was extracted and quickly frozen by wrapping it in parafilm then burying the tissue in dry ice until thoroughly frozen (approximately 5-10 minutes). The brain was then oriented and

mounted using Optimal Cutting Temperature (O.C.T) medium rostral side down. A Thermofisher (Fairelawn, NJ) cryostat maintained at low temperature (-20°C) was used to section the brain tissue into 40 micron sections and mounted on poly-L-lysine coated positively charged slides.

Prior to antibody staining, the slides were first post-fixed in a solution of 4% paraformaldehyde in a 50/50 mix of absolute ethanol and water for 2 minutes. Slides were then transferred into a light protected moisture chamber (Newcomer Supply, Middleton, WI) and treated with a 3% donkey blocking serum (Jackson Immuno Research, West Grove, PA). The donkey serum was prepared in 1x PBS with 0.5% Triton X-100 (Sigma Aldrich, St. Louis, MO). The blocking serum is removed without rinsing the slides. Next, the slides are treated with dopamine receptor (DRD2) primary antibody (Alomone Labs, Jerusalem, Israel) at a 1:100 dilution prepared with 1% donkey serum, 0.3% Triton X-100. The slides were covered with a coverslip and sealed with rubber cement; then left to incubate in the primary antibody for 48 hours in the refrigerator. Following incubation, the rubber cement was peeled off and the slides were thoroughly washed with 1x PBS five times, or approximately 10 minutes. The secondary antibody was prepared at a 1:500 dilution in 1% donkey serum and 0.3% Triton X-100 and incubated for one hour at room temperature. After treatment with the secondary antibody, slides were again washed with 1x PBS for another 10 minutes, or five times. Then slides were mounted with Fluoromount (Southern Biotech, Birmingham, AL) and coverslipped. Following the antibody incubation, slides were visualized with a fluorescence confocal microscope (Oberkochen, Germany), and representative images were taken to identify the anatomical areas of interest, and dopamine receptors were analyzed.

3.6. Data Analysis

Fast Scan Cyclic Voltammetry (FSCV) analysis was performed using the High Definition Cyclic Voltammetry (HDCV) Analysis software. Pre-calibrations were gathered before the experiment, performed in quadruplicate, then used to generate a calibration factor by dividing the monoamine standard concentration by the average peak current. The standards were captured, which included their cyclic voltammogram, and was used to train the software in coordination with the calibration factor to match the same corresponding voltammogram pattern that presents in the data file. The training set converted any matching signal from the standards and translated it into a current versus time plot. Signals not determined from the training set, such as artificial stimulation artifacts or interfering analytes, were not represented. Peak current signals were automatically converted to concentration which could then be extracted and examined statistically.

Immunocytochemistry quantifications were performed using ImageJ software (Bethesda, MD). Slide images were cropped to only include the brain region of interest. The image was then converted to grayscale in order to maximize the contrast between pixel signals. Any background from the staining was corrected by shifting the scale to auto max and applying a dark background. Only representative pixels will then appear, which are associated with positive receptor staining. The software provided the appropriate count of the pixels that were present.

CHAPTER 4

RESULTS

4.1 Fast Scan Cyclic Voltammetry System
Design and Validation

Fast scan cyclic voltammetry stands as an elegant tool for detecting and quantifying

neurochemicals within a complicated biological environment. Due to the complications inherent

in taking these measurements, the FSCV system must be adequately calibrated and validated.

Herein, dopamine and potential interfering agents, such as ascorbic acid were measured with a

flow-cell based FSCV.

4.1.1 Calibration with Dopamine

Dopamine is the primary analyte in this project. A series of dopamine standards were

prepared in the calibration artificial cerebrospinal fluid outlined under the methods section 3.4.3.

Measurements were gathered via flow cell injection and application of electrical potential in a

triangular waveform extending from -0.4 to +1.3 V and back to -0.4 V at a scan rate of 400 V/s

at a carbon fiber microelectrode surface. The flow cell measurements provided cyclic

voltammograms of the dopamine standards from 100 to 700 nM in 100 nM increments (Figure

15 A). Dopamine is known to oxidize at ~ 0.6 V and reduces at ~ -0.2 V, as indicated by the

figure 16A. The shape of the voltammogram also provides a confirmation of the analyte. At

increasing concentration, the peak current demonstrates an equivalent increase. To examine the

full extent of the linear relationship between the peak current and concentration, the peak current

was plotted against the standard dopamine concentration (Figure 15 B).
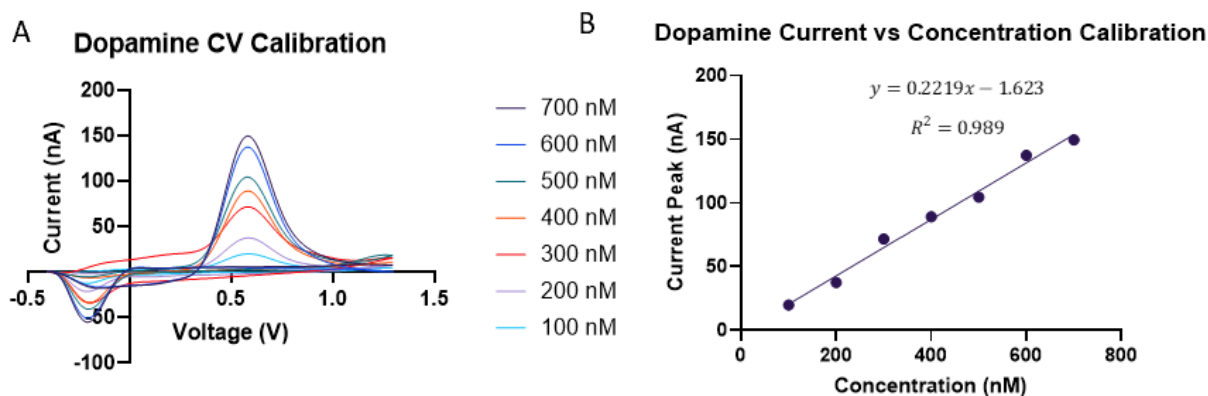
Figure 15. Dopamine calibration using flow cell FSCV. (A) Dopamine cyclic voltammogram of standards relating increasing peak current with increasing concentration. (B) Dopamine calibration curve with linear regression and correlation applied.

A linear regression of the relationship between dopamine peak current and the concentration of the flow cell injected standards was performed. The equation of the line was obtained to be y = 0.2219x – 1.623 with coefficient of determination, R^2 of 0.989, suggesting a good linear correlation between the instrumental response and concentration (Figure 15 B). Based on the data derived from the calibration curve the limit of detection ($LOD = 3.3 * \frac{slope}{standard\ deviation}$) and limit of quantification ($LOQ = 10 * \frac{slope}{standard\ deviation}$) can be calculated as 0.2 nM and 0.5 nM, respectively.

4.1.2 Ascorbic Acid Calibration

Ascorbic acid is a naturally occurring antioxidant that can also be found in significant quantities in the brain, commonly presenting as the chief interfering analyte in neurological measurements; accounting for and characterizing the presence of ascorbic acid becomes essential. Ascorbic acid demonstrates a single oxidation peak at approximately 0.6 V and so a triangular waveform was applied, ranging from -1.0 to +0.8 V, to encompass the full electroactive range of the analyte. Like the dopamine calibrations, the ascorbic acid calibration was performed through a flow cell injection of 1 to 10 mM ascorbic acid standard with 1 mM

increments. An overlay of the voltammograms were generated according to the increasing

concentrations (Figure 16 A).

A

Ascorbic Acid CV Calibration

B

Ascorbic Acid Calibration Current vs Concentration
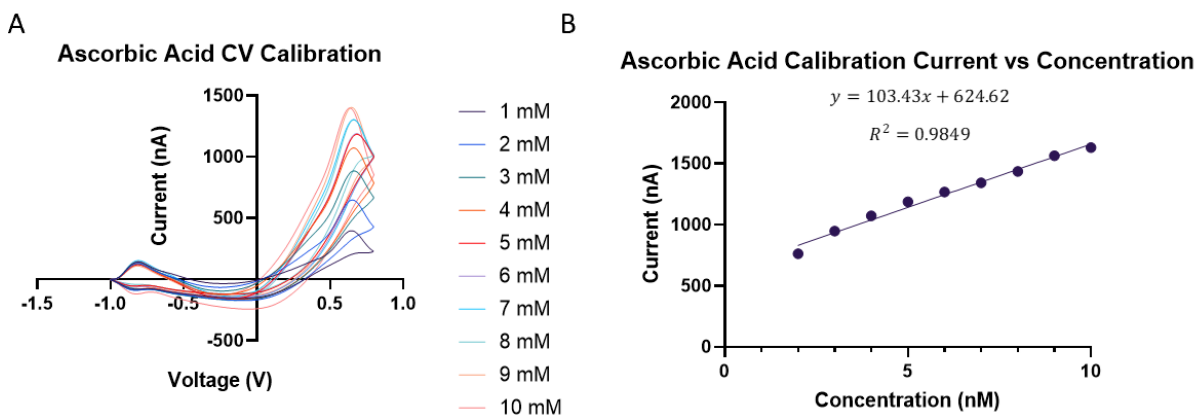
Figure 16. Ascorbic acid calibration by flow cell FSCV. (A) Cyclic voltammogram overlay of ascorbic acid standards denoting changes in peak current with increasing standard concentration. (B) Ascorbic acid calibration curve with linear regression and correlation analysis applied.

The peak current generated from the flow cell injections were plotted against the

concentration of the standards. A linear regression analysis was performed. The equation of the

line was obtained to be $y = 103.43x + 624.62$ with coefficient of determination, R^2 of 0.9849,

suggesting a good linear correlation between the instrumental response and concentration (Figure

16 B). Based upon the data derived from the calibration curve the limit of detection ($LOD =$

$3.3 * \frac{slope}{standard\ deviation}$) and quantification ($LOQ = 10 * \frac{slope}{standard\ deviation}$) were determined to

be 1.2 nM and 4.8 nM, respectively.

4.1.3 Dopamine/Norepinephrine Calibrations

Aside from dopamine and ascorbic acid, norepinephrine displays electroactivity along the

same waveform potential. Additionally, stimulation events may produce the release of a

multitude of different neurochemicals simultaneously. Dopamine and norepinephrine belong to

the monoamine classification and, as such, are synthesized through the same process with

norepinephrine being downstream of dopamine. A mixture of dopamine and norepinephrine was examined to see if the system could discriminate between the two monoamines. The same calibration procedure for dopamine, including the waveform parameters for was employed for the combination mixture. The dopamine-norepinephrine mixture had concentrations ranging from 200 to 1000 nM by 200 nM increments. An overlay of the voltammograms were produced (Figure 17 A) to demonstrate the different shape and distributions of the redox potentials for the combination analytes. Dopamine's peak oxidation remained at ~ +0.6V and was utilized in the generation of the calibration curve. The oxidation peak for norepinephrine appears at ~ +0.2V.
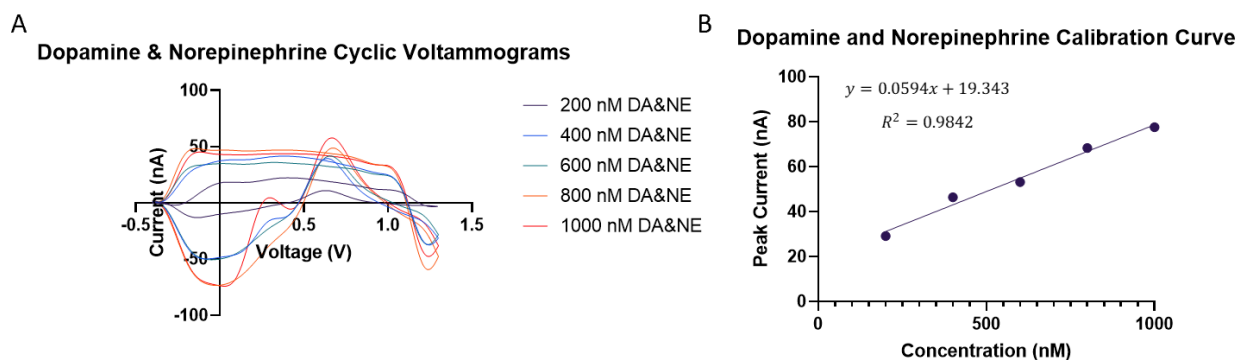
Figure 17. Flow cell FSCV of dopamine and norepinephrine in mixture. (A) Voltammogram overlay of dopamine and norepinephrine mixture indicating an increasing trend between peak current for dopamine and the concentration. (B) Calibration curve of dopamine peak current versus the concentration of the dopamine-norepinephrine standards.

The peak oxidation current for dopamine from the flow cell measurements of the mixture was plotted against the concentrations of the mixture (Figure 17 B). A linear regression of the relationship between the combinations of both dopamine and norepinephrine peak current and concentration of the flow cell injected standards was performed. The equation of the line was obtained to be $y = 0.0594x + 19.343$ with a coefficient of determination, R^2 of 0.9842, suggesting a good linear correlation, indicating a robustness of the dopamine signal in the presence of another monoamine (Figure 17 B).

4.2 Fast Scan Cyclic Voltammetry Analysis
in Brain Slices

The optimum parameters established with the flow cell FSCV were utilized in the slice

FSCV. The data obtained were in the form of pseudo color plots, current vs time plots, and cyclic

voltammograms.

4.2.1 Measuring Dopamine in
the Inferior Colliculus

A typical cyclic voltammogram for dopamine has a single oxidation peak at ~ +0.6 V and

reduction peak at ~ -0.2 V, corresponding to the green and blue colors, respectively in the pseudo

color plot (Figure 18 C & D). However, the data obtained from the slice FSCV measurement

from the inferior colliculus resulted in a voltammogram with two distinct oxidation peaks at ~ -

0.2 and +1.0 V and one reduction peak at +0.15 V. The corresponding pseudo color plot (Figure

18 A & B) also reflects the emergence of both oxidation peaks. By comparing the slice FSCV

data with the expected voltammogram (Figure 18 A & B versus C&D), it is obvious that two

electroactive species are being detected simultaneously from the slice measurement.
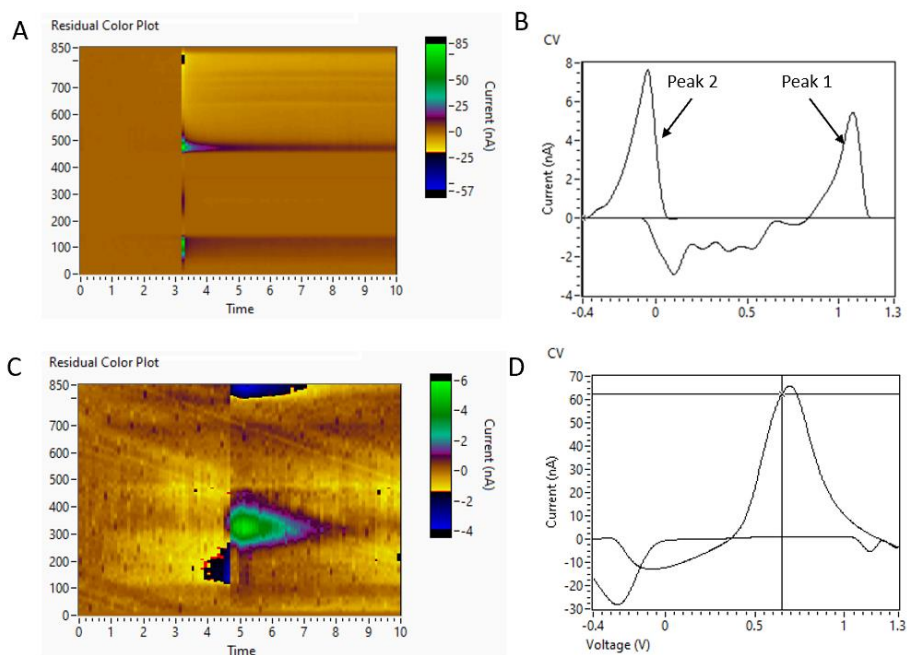
Figure 18. Sample of slice FSCV color plots and voltammograms. (A) Color plot from control subject, indicating two separate oxidation peaks in green. (B) Corresponding cyclic voltammogram displaying the two oxidation peaks (1 & 2). (C) Example of an expected color plot for dopamine, with (D) corresponding cyclic voltammogram.

Since the waveform applied can initiate redox reactions from other monoamines, the most likely suspect of the secondary peak is another monoamine. Norepinephrine has the same redox window as dopamine and could be a reasonable candidate for the secondary signal. The FSCV software can generate training sets from flow cell injected standards to produce a signal that can be useful for identification purposes. The dopamine and norepinephrine mixture was analyzed through the flow injection system and a training set was generated through a K-Matrix algorithm (Figure 19 A). A comparison of the K-Matrix training set with the corresponding pseudo color plot for the flow cell injected dopamine-norepinephrine standard versus the slice FSCV data suggests simultaneous detection of the two monoamines in the slice measurement (Figure 19).
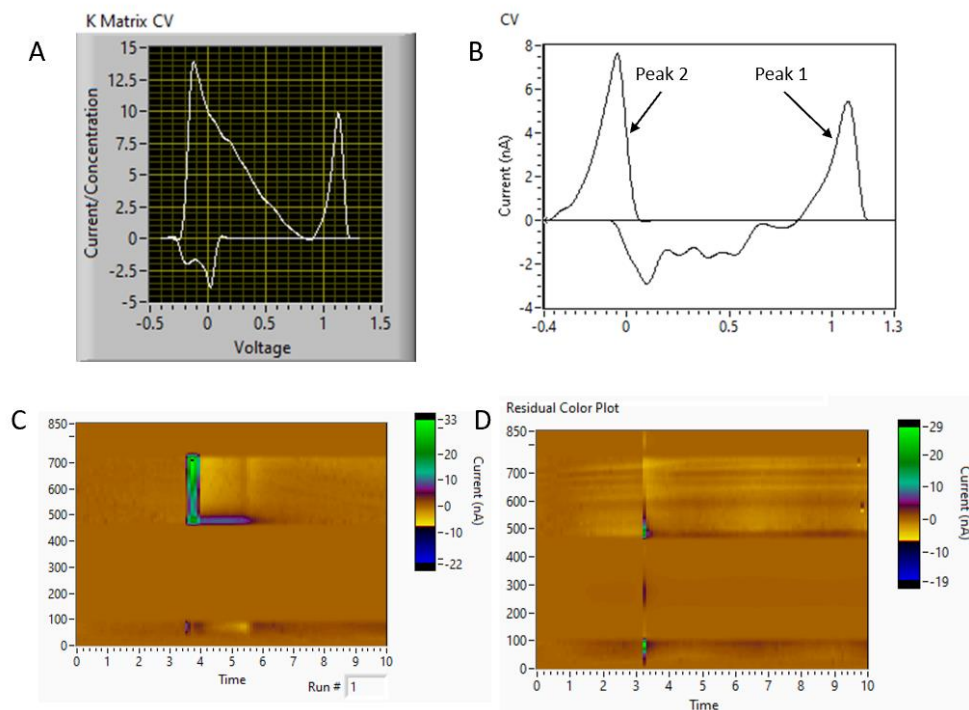
Figure 19. Comparison of the data from flow cell injected dopamine-norepinephrine standards with the slice FSCV data. (A) K-Matrix analysis of the predicted cyclic voltammogram for the dopamine-norepinephrine standard solution. (B) Cyclic voltammogram for the slice FSCV demonstrating similarity with the K-Matrix prediction. (C) Flow cell-produced pseudo color plot for dopamine-norepinephrine standard solution. (D) Pseudo color plot for the slice FSCV.

Peak current can be converted into concentration through the application of a calibration factor. This conversion was determined through pre-calibration measures of several runs of the neurochemical standard, either dopamine or norepinephrine, and then calculating the calibration factor in terms of nA/nM. Thus, the current vs time traces can be converted into a concentration vs time trace. The two suspected monoamine peaks plotted for both current vs time (Figure 20 A) and concentration vs time (Figure 20 B). Each of the peaks between were distinct and independent of the other, suggesting that they are not just artifact signals.

A

Peak Current vs Time

B

Concentration vs Time
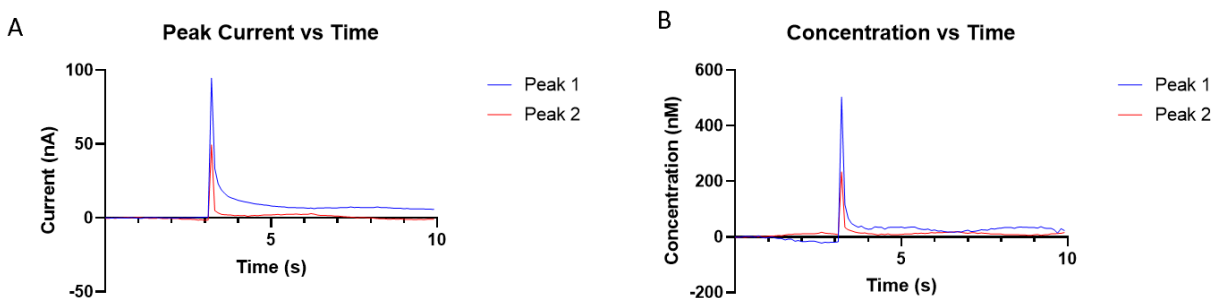
Figure 20. Comparisons of peak 1 and 2 neurotransmission events in a control subject. (A) Current vs time trace between peak 1 and 2. (B) Concentration vs time trace between peak 1 and 2.

Peak 1 was further examined with the analysis software using Fourier transformations to isolate the signal from peak 2. This transformation was possible in part due to the peak 1 having a higher concentration than peak 2. Peak 2 was filtered out using the transformation and was absent in the newly generated color plot (Figure 21 A). Further analysis of the transformed voltammogram reveals a close resemblance to the cyclic voltammogram of dopamine standard, with a reduction peak appearing at -0.25 V and an oxidation peak slightly right shifted at +1.0 V (Figure 21 B). Additional attempts at transforming the lower peak could not be achieved without dropping the total signal.
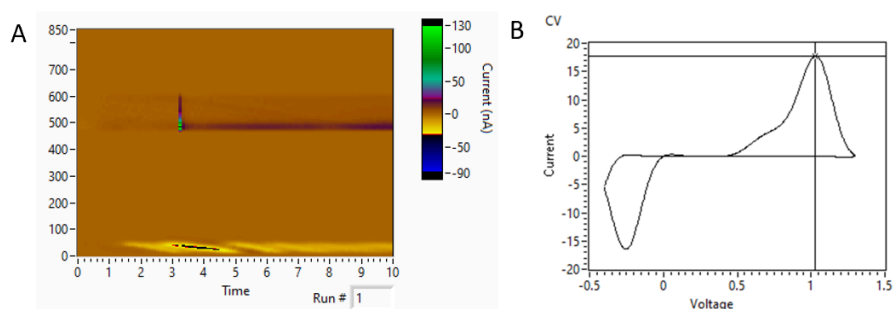
Figure 21. Fourier Transformation of the slice FSCV data. (A) Pseudo color plot of Fourier transformed data depicting the now singular oxidation peak. (B) Cyclic voltammogram of Fourier transformed data displaying a more traditional dopamine CV.

**4.2.2 Pharmacological Verification
of the Identity of the Slice Fast
Scan Cyclic Voltammetry Data**

The analysis presented by the K-Matrix and the Fourier transformations provides the first

supporting evidence towards identifying two signals in the FSCV data. Pharmacological agents

can be used to selectively target the specific sections of the neurochemical pathway through

either activation or inhibition of specific receptors, or proteins that could aid in the identification

of the signals.

4.2.2.1 Tetrabenazine

Tetrabenazine (TBZ) is a hexahydro-dimethoxy-benzoquinolizine derivative that operates

as a monoamine, depleting drug by blocking the vesicular monoamine transporter 2 (VMAT2),

which is responsible for packing monoamines, such as dopamine and norepinephrine into their

respective vesicles (Yero & Rey, 2008). Varying concentrations of TBZ was added to the

oxygenated aCSF running buffer perfusing through the slice FSCV recording chamber after

obtaining a stable signal from the brain slice. The effect of each dose of TBZ on the signal was

measured every 5 minutes for 30 minutes.
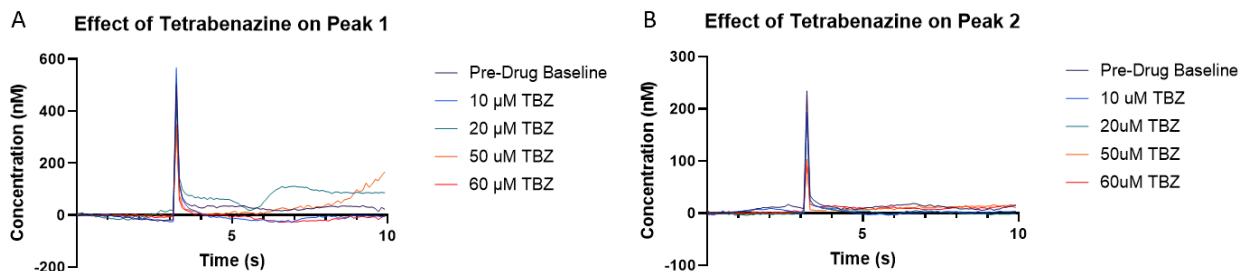
Figure 22. Effect of TBZ on the slice two FSCV signals measured from the inferior colliculus.
(A) Peak 1 concentration decreases with increasing dose of TBZ perfused through the recording
chamber. (B) Peak 2 concentration also decreases with increasing dose of TBZ. The data
confirms the two peaks to be monoamines.

The peak current from the current vs time trace was converted to concentration using the pre-calibration factors for both monoamine standards. Each peak demonstrated a decrease in the concentration of the release event with increasing concentration of tetrabenazine, thus suggesting the two peaks are monoamines (Figure 22). The effectiveness of the drug can be determined through examining the resulting drug influence. Since the drug operates through an inhibitory mechanism, the drug's efficacy is described as an IC50. Which means the concentration at which the drug inhibited 50% of the response. The IC50 was determined from a plot of the logarithmic transformation of the concentrations of tetrabenazine versus the normalized FSCV signal. The concentration of tetrabenazine that reduced the release signal for peak 1 in the inferior colliculus by 50% was calculated to 6.62 µM (Figure 23 A) with a correlation coefficient of 0.9827. The amount of tetrabenazine needed to reduce the release signal for peak 2 by 50% was determined to be 36.5 µM (Figure 23 B) and a correlation coefficient of 0.6400.
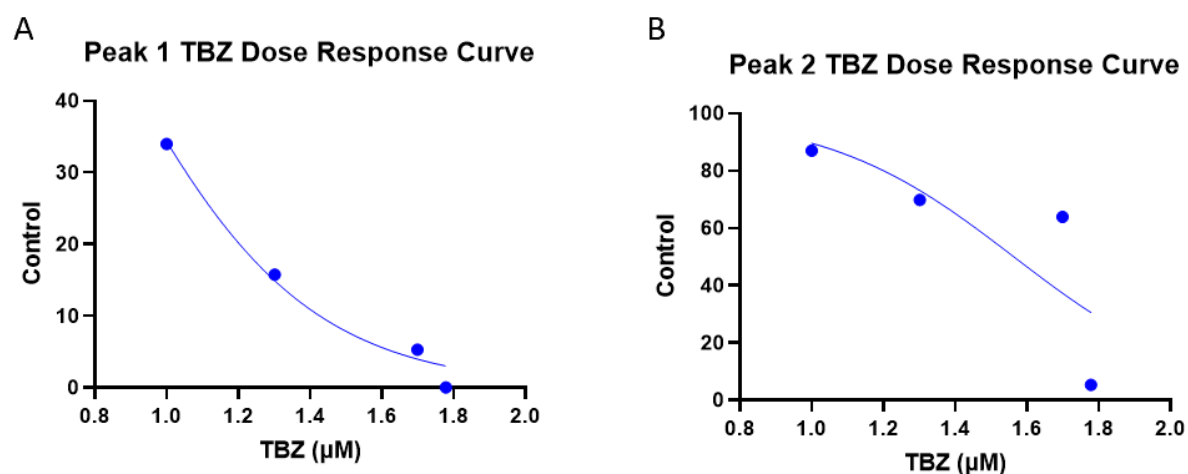
Figure 23. Dose response curve depicting the IC50 values for TBZ for peak 1 and peak 2 signals recorded from the inferior colliculus. (A) IC50 for peak 1 dose respond curve relating an effective concentration of TBZ at 6.62 µM. (B) IC50 of peak 2 relating the effective concentration of TBZ at 36.5 µM.

4.2.2.2 Quinpirole

The current pharmacological experiments have demonstrated the two peaks to be signals from monoamine neurotransmission, however, to further identify the peaks another round of pharmacological studies was performed. Quinpirole operates as a dopamine D2/D3 receptor agonist which, in turn, triggers the inhibitory effects of the dopamine autoreceptors (Eagle et al., 2014). Thus, perfusions with quinpirole are expected to decrease the concentration of dopamine release, while leaving the signals from monoamines, like norepinephrine, unaffected.

Quinpirole perfusion was performed using the same procedure as TBZ. The drug perfusion began following a stable baseline signal starting with a dose of 0.001 μM and increased by one order of magnitude over the course of 30 minutes of perfusion before ending at a final quinpirole concentration of 10 μM; with voltametric recordings being taken every 5 minutes for 30 minute per dose of the drug. The stimulated current was converted into concentration according to the procedure as already described.
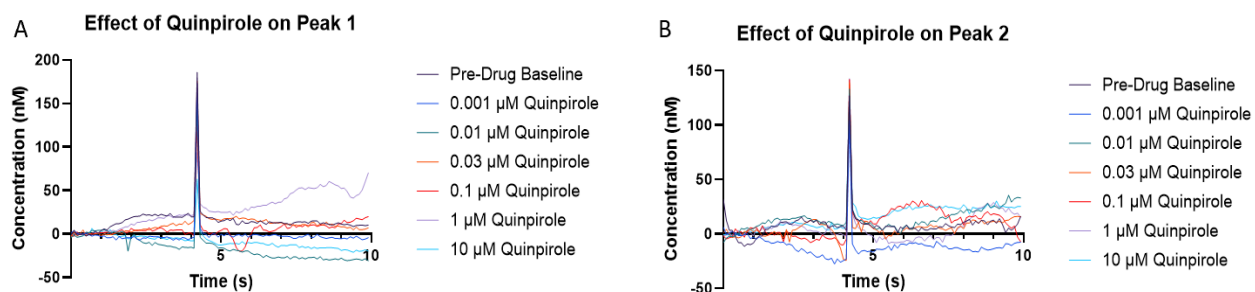
Figure 24. Effect of quinpirole on monoamine release. (A) Concentration vs time traces for peak 1 demonstrating decrease release per increasing quinpirole concentration. (B) Peak 2 signal was not significantly impacted by the varying dose of quinpirole.

The concentration of peak 1 signal displayed a clear and consistent decrease across increasing quinpirole concentrations (Figure 24 A). The effects of quinpirole on peak 2 concentrations only displayed minor fluctuations but remained otherwise unchanged (Figure 24 B).

An IC50 analysis was performed to assess the effective inhibitory concentration for both peaks. The effective inhibitory concentration of quinpirole for reducing the peak concentration of peak 1 was 9.65 x10^{-3} μM (Figure 25 A). The correlation coefficient was 0.9703. The IC50 for the peak 2 control groups were tabulated to be 2.47 x 10^{30} μM (Figure 25 B). The correlation coefficient for both control groups was 0.0006.

A

B
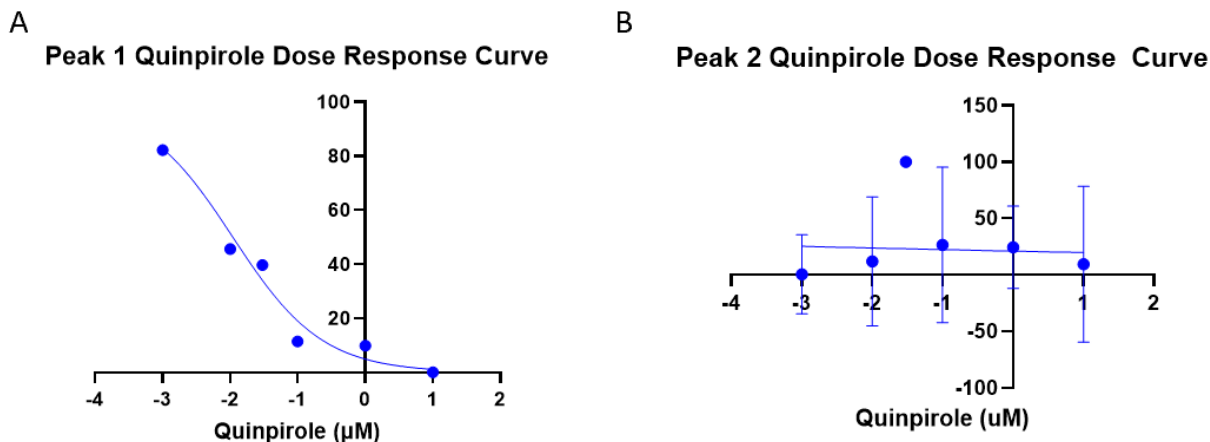
Figure 25. Dose response curve for quinpirole's action on the two monoamines. (A) Analyzing quinpirole's effect on the release concentration of peak 1. (B) Quinpirole's effect on the release concentration of peak 2.

4.2.2.3 Sulpiride

Sulpiride is a selective antagonist for dopamine D2 receptors that is also reported to block D3 and D4 receptors (Caley & Weber, 1995). While quinpirole operates to reduce the overall output of dopamine from target neurons, sulpiride acts much in the opposite fashion. Since D2 receptors are inhibitory, blocking their activation leaves more dopamine within the synapse, ultimately leaving an overall net increase in dopamine release. Sulpiride is often included in experiments that are treated first with quinpirole to restore functionality of the receptor following the activations from quinpirole.

Sulpiride perfusions were performed following the previous quinpirole experiments outlined in section 4.3.3. After the final quinpirole concentration had been perfused, the running

aCSF buffer was replaced with fresh running buffer for 10 minutes to clear the lines, then a new solution with 0.001 μM sulpiride was perfused over the brain slice in the recording chamber for 30 minutes. The sulpiride concentration was increased, replicating the same doses as the quinpirole experiment. The sulpiride dose was perfused for 30 minutes with voltammetry recordings being taken every 5 minutes.

Peak 1 concentration was either very low or near 0 following the quinpirole drug perfusions. Initiating cumulative doses of sulpiride demonstrated increases in peak 1 concentrations (Figure 26 A). The effect of sulpiride on peak 2 displayed minor fluctuations the concentration of the signal (Figure 26 B).
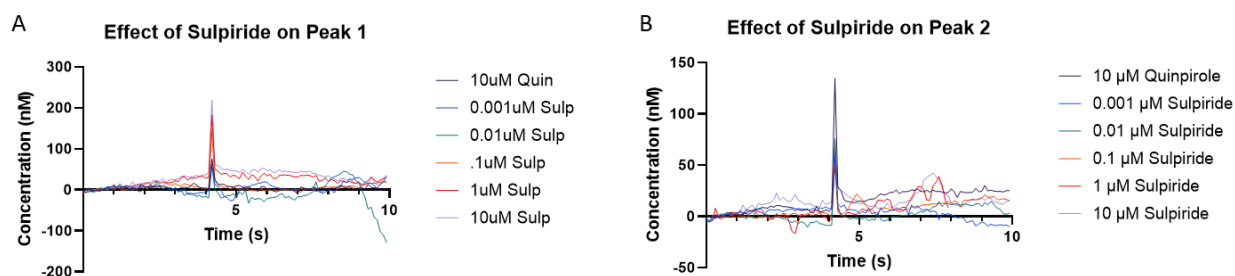
Figure 26. Effect of sulpiride on monoamine release. (A) Peak 1 concentration increases with increasing sulpiride dose. (B) Impact of sulpiride perfusion on the concentration of peak 2.

An EC50 analysis was performed to assess the effective concentration to which 50% response was elicited by the drug. The effective concentration of sulpiride on peak 1 concentration was 0.989 μM (Figure 27 A). The correlation coefficient for the peak 1 was 0.7956. The EC50 for peak 2 was 0.264 μM (Figure 27 B), with a corresponding correlation coefficient of 0.2651.

A

Peak 1 Sulpiride Dose Response Curve

B

Peak 2 Sulpiride Dose Response Curve
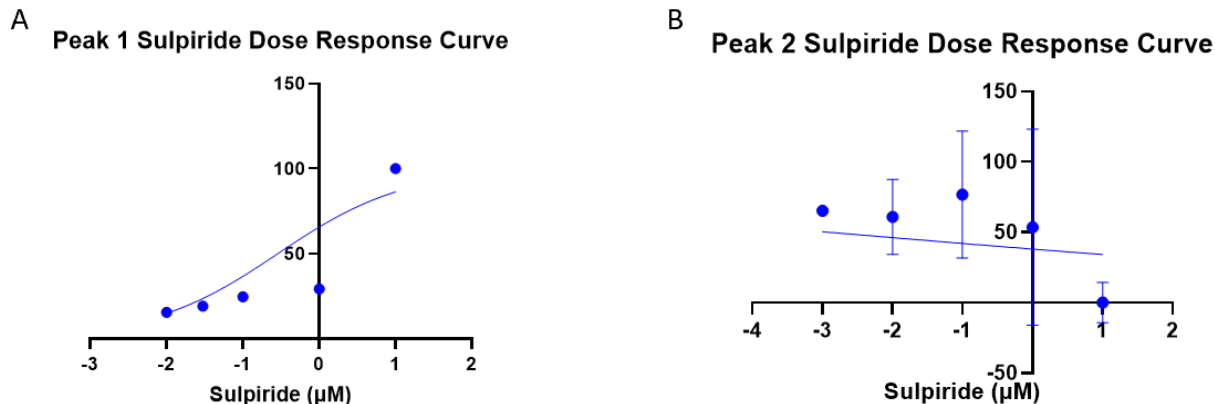
Figure 27. Sulpiride dose response curve. (A) The effect of sulpiride on peak 1 concentration. (B) The effect of sulpiride on peak 2 concentration.

4.2.2.4 7-Hydroxy-N,N-dipropyl-2-aminotetralin

The final pharmacological agent utilized in this study was 7-hydroxy-*N,N*-dipropyl-2-aminotetralin (which will be referenced as 7-OH-DPAT for the remainder of the document). 7-OH-DPAT acts as a selective agonist for D3 dopamine receptors. Similarly, to D2 dopamine receptors, D3 receptors yield an inhibitory effect on dopamine neurotransmission. Additionally, there is evidence that 7-OH-DPAT will also influence inhibition of norepinephrine release (Chu et al., 2004). Perfusions of the drug continued with the same procedure and concentrations as the previous pharmacological agents.

Measured monoamine release events had their peak currents converted into concentration. Peak 1 concentration decreased over the course of the experiment with increasing 7-OH-DPAT concentrations (Figure 28 A). Peak 2 concentration had some fluctuations present, but overall maintained a relatively consistent level throughout the course of the experiment (Figure 28 B).
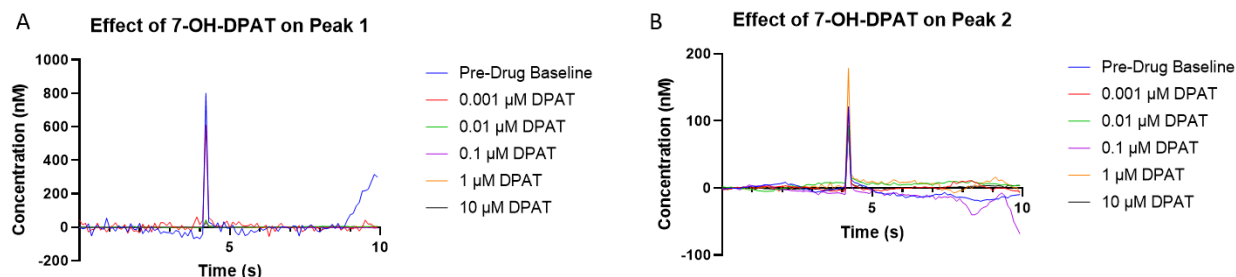
Figure 28. Effect of **7-OH-DPAT** on monoamine release. (A) Peak 1 concentration decreased with increasing concentrations of 7-OH-DPAT. (B) Peak 2 concentration maintains a relatively consistent value with increasing 7-OH-DPAT concentration.

7-OH-DPAT's effectiveness was further examined using the IC50 metric. The effective

concentration of 7-OH-DPAT was determined to be 0.001 μM for peak 1 and 0.0001 μM for

peak 2 (Figure 29). The correlation coefficients for each IC50 determination was 0.9554 for peak

1 and 0.002059 for peak 2.
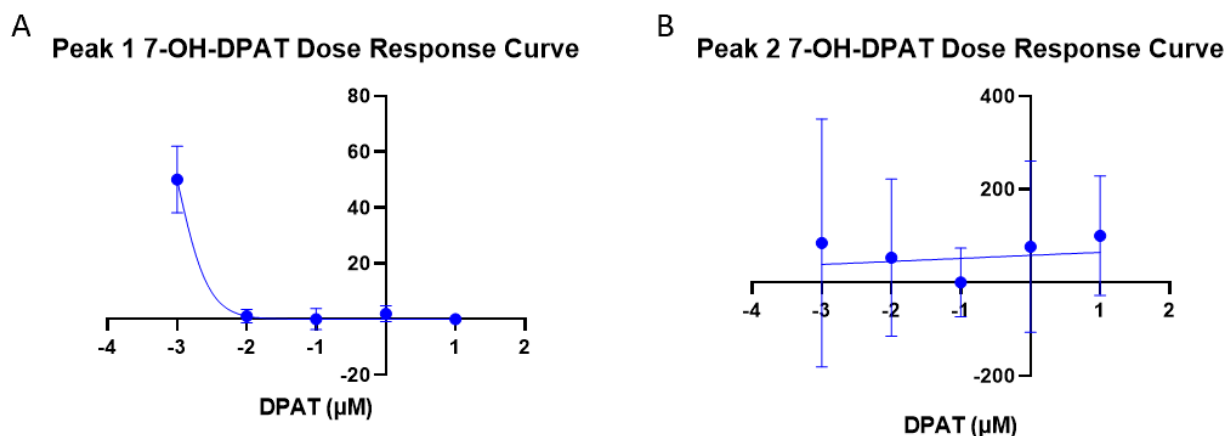
Figure 29. 7-OH-DPAT dose response curves. (A) Effective drug dose of 7-OH-DPAT on peak 1 was 0.001 μM. (B) Effective drug dose of 7-OH-DPAT on peak 2 was 0.0001μM.

The combined results from each of the pharmacological experiments indicate that both

peaks are monoamines. Peak 1 demonstrated extensive modulation with dopamine related

agonists and antagonists and can reliably be identified as dopamine. The second peak displayed

consistent resistance to specific dopamine targeting drugs, while also being affected by general

monoamine inhibitors. According to the monoamine synthesis pathway, the most likely identity of the second peak is norepinephrine.

4.2.3 Effect of Noise Exposure on Monoamine Neurotransmission

The previous experiments have established the presence of two monoamines, dopamine, and norepinephrine in the inferior colliculus. The effect of loud noise on the release of these monoamines was examined. Analysis of tissues obtained from the noise exposed subjects was conducted 24-hours after the exposure to ensure that changes measured were real and not just transient reactions to the discomfort of the noise exposure, and to also allow adequate time for possible compensatory response.

The two peaks observed in the control subjects persisted also in the noise exposed subjects. By inspection, the dopamine peak for the noise exposed subjects were markedly attenuated compared to their control, an effect that was also consistent with the norepinephrine (Figure 30).
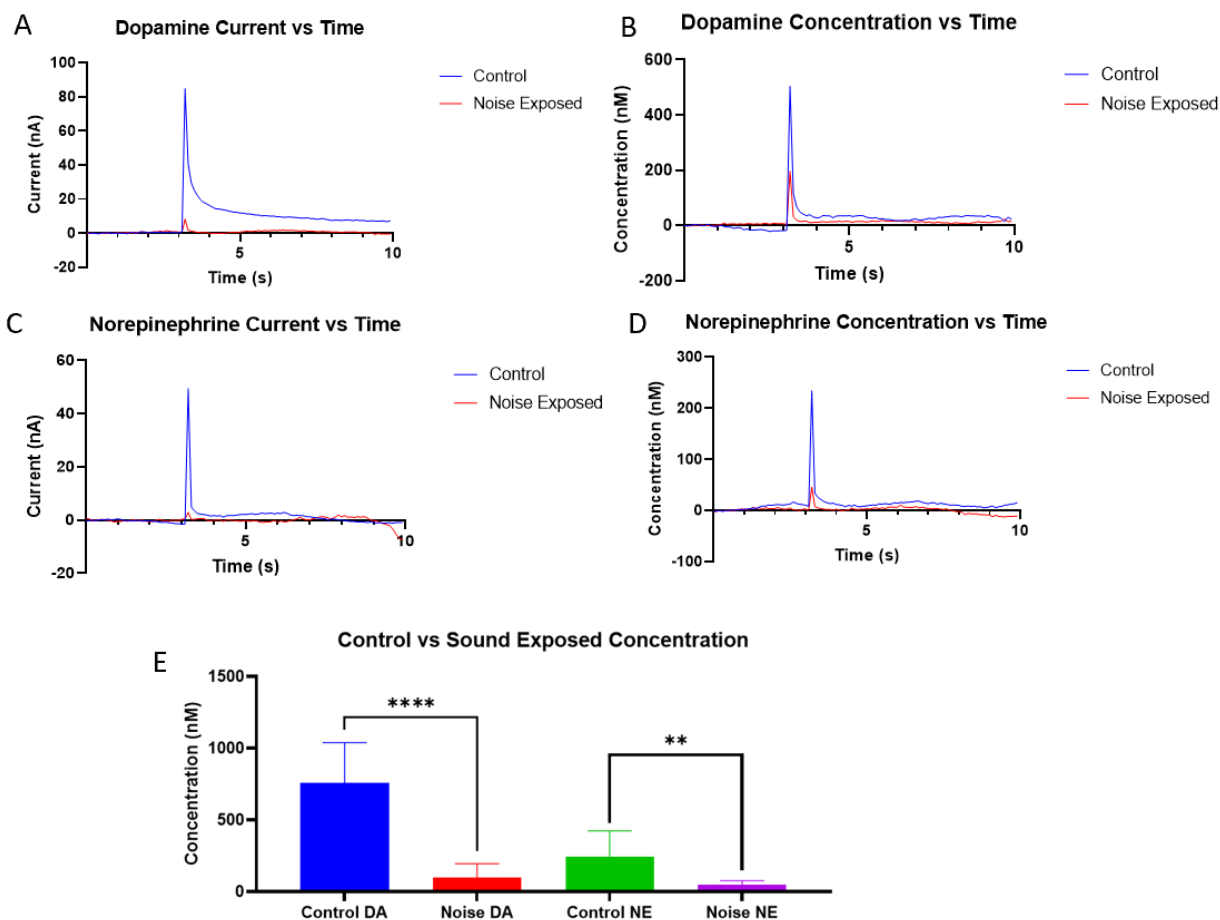
Figure 30. Comparison of monoamine release in the inferior colliculus of control vs noise exposed subjects. (B) Dopamine concentration vs time trace. (D) Norepinephrine concentration vs time trace. (E) Exposure to loud noise decreases dopamine and norepinephrine release in the inferior colliculus. Unpaired t-tests between control and noise exposed groups for dopamine and norepinephrine were performed. Effects of loud noise was found to be statistically significant for dopamine (p-value = 0.0004) and norepinephrine (p-value = 0.003).

To evaluate the significance of the effects of noise on the monoamine release in the inferior colliculus, a set of unpaired t-tests were performed to compare the control subjects with the noise exposed counterparts. The effects of loud noise on dopamine and norepinephrine release was found to be statistically significant, $t(10) = 5.207$, p-value = 0.0004; and $t(13) = 3.654$, p-value = 0.003, respectively (Figure 30 E).

Furthermore, several noise exposed subjects were left to recover for two additional days as a confirmatory measure to determine if the effects of the noise exposure were permanent. From an N = 3, a comparison among the monoamine groups produced an average dopamine release concentration of 573.2 nM for the control group, 199.3 nM for the noise exposed +1 days recovery group, and 81.80 nM for the noise exposed +3 days recovery group. The average norepinephrine release concentration for the control group was 266.0 nM, 45.98 nM for the noise exposed +1 days recovery group, and 31.45 nM for the noise exposed +3 days recovery group. Each indicates that the damage in the neurotransmission incurred from the noise exposure was long lasting (Figure 31).
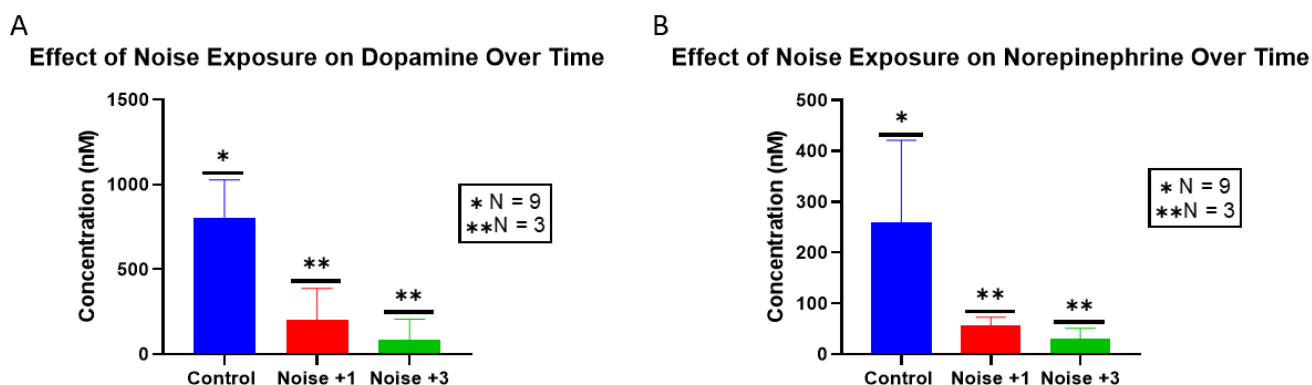
Figure 31 Comparison of the effect of loud noise on monoamine neurotransmission over time. (A) Dopamine release in control versus noise exposed groups. (B) Norepinephrine release in control versus noise exposed groups. Noise +1: represent noise exposed subjects with 1 day recovery time before analysis, Noise +1: represent noise exposed subjects with 3 days recovery time before analysis.

4.2.4 Pharmacological Studies on Noise Exposed Subjects

Similar to the control groups, pharmacological perfusions were used to further examine the dynamics of the inferior colliculus following drug noise exposure. These experiments followed in line with the previous pharmacological studies. While the dopamine peak was influenced by a variety of pharmacological manipulations, norepinephrine remained unchanged throughout and will instead be reported in Appendix B.

Alpha-methyl-p-tyrosine (AMPT) is another pharmacological agent that operates as a catecholamine inhibitor, specifically acting upon the monoamine synthesis pathway by inhibiting the hydroxylation step, converting tyrosine to L-DOPA (Brogden et al., 1981). Tetrabenazine inhibits VMAT2, which packages monoamines into their vesicles following synthesis to be released upon action potential at the axon terminal, AMPT is often used in conjunction with tetrabenazine to probe the synthesis process. Both drugs were included as a single cocktail to diminish the monoamine signal more effectively. Tetrabenazine was introduced to the brain slice alone for the first trial, then for each subsequent collection, AMPT was added and held constant at 50 µM for the remainder of the experiment. The concentration of tetrabenazine was then increased to 25 µM and 140 µM for each subsequent trial. Additionally, each of the previous drug trials were repeated on noise exposed subjects and the effects of the drugs were analyzed using their respective dose response parameters.

The combination of tetrabenazine and AMPT displayed a more definitive reduction in overall dopamine release signal than the control experiments where tetrabenazine was used alone. The drug combination generated an effective 50% dose response at concentration 1.302 µM (Figure 32 A). A repeat of quinpirole and sulpiride on the noise exposed groups displayed a visually close response compared with the control experiments. The effective dose concentration was calculated as 0.01328 µM for quinpirole (Figure 32 B) and 0.1618 µM for sulpiride (Figure 32 C). 7-OH-DPAT appeared slightly different than the control counterpart, delivering an effective dose concentration of 0.02298 µM (Figure 32 D).
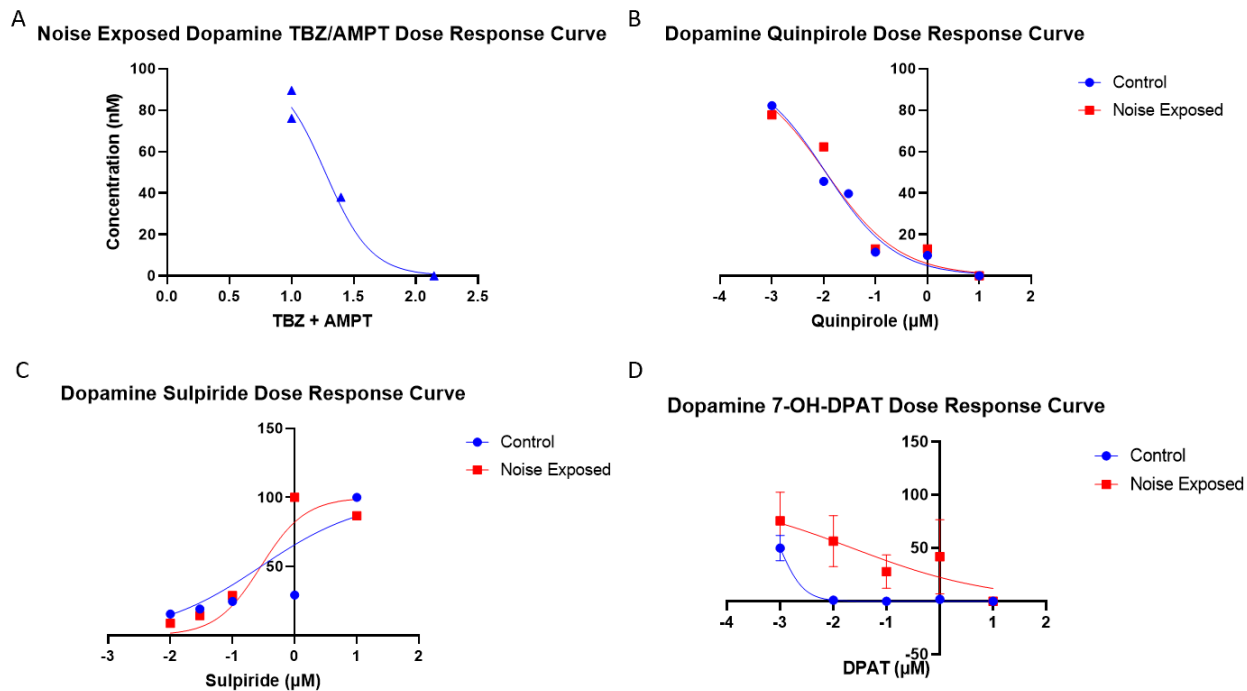
Figure 32. Pharmacological manipulated dose response curves on noise exposed dopamine release. (A) TBZ/AMPT cocktail relays an effective drug concentration of 1.302 µM. (B) Quinpirole IC50 effective drug concentration of 0.01328 µM. (C) Sulpiride EC50 effective drug concentration of 0.1618 µM. (D) 7-OH-DPAT IC50 effective drug concentration 0.02298 µM.

To determine if the effects of the noise exposure impacted the receptor pathway, a series of unpaired t-tests were performed. A comparison of the effectiveness of quinpirole between both experimental groups displayed a lack of statistical significance, $t(12) = 1.239$, p-value = 0.2391. Sulpiride continued to demonstrate a similar lack of statistical significance as well, $t(13) = 1.019$, p-value = 0.3266. 7-OH-DPAT displayed a slightly different pattern than the other dose response curves, however, the unpaired t-test found the difference between the control and noise exposed groups to be borderline significant, $t(11) = 2.134$, p-value = 0.0562.

**4.3 Assessing the Impact of Noise on Dopamine Receptor
Distribution in the Inferior Colliculus**

Immunocytochemistry was used to examine the impact of loud noise on the dopamine

receptor distribution in the inferior colliculus. Brain slices were mounted and stained, as outlined

in section 3.6.1 of chapter 3. The images of brain slices were composited through a stitching

feature in the confocal microscope's software to generate a complete coronal cross section of the

slice. Areas of the tissue morphology were assessed in coordination with the Paxinos Rat Atlas to

establish a commonality among each of the tissue sections, so an appropriate comparison could

be made among the control versus noise exposed groups (Figure 33 A). Stained brain sections

utilized Alexa Fluor 488 providing the distinctive green fluorescence (Figure 33 B), and a closer

zoom of the tissue demonstrates an example of the brighter neural cell bodies present (Figure 33

C).
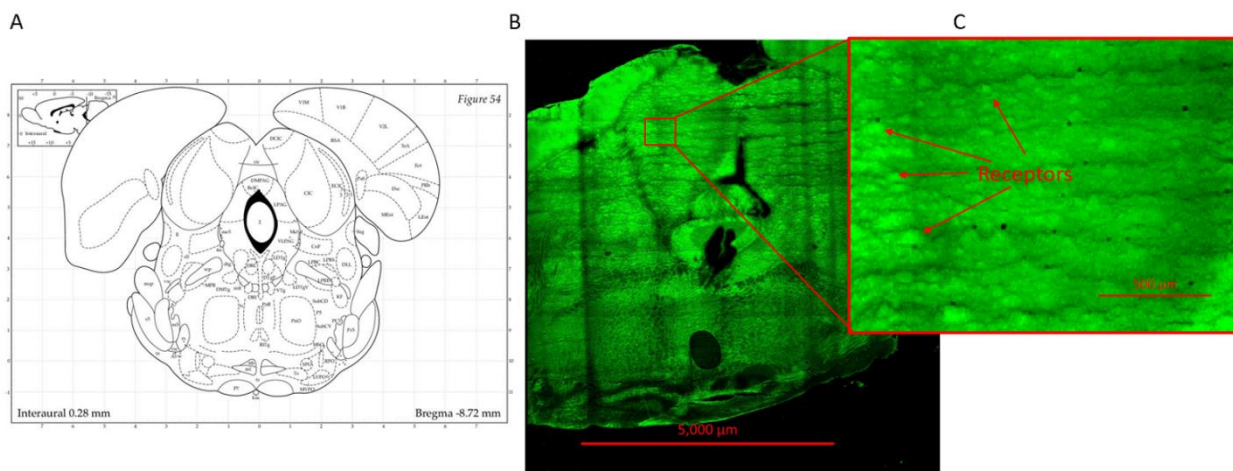
Figure 33. Coronal brain section of the inferior colliculus. (A) Rat brain atlas showing the
region of interest (Paxinos & Watson, 2013). (B) Image of a stitched immunocytochemistry-
stained section of rodent brain and (C) zoomed region depicting neuron cell bodies. Green:
Alexa Fluor 488.

Each of the stained sections were processed and analyzed using ImageJ software (NIH),

which selectively attributes positive pixel signals with positive antibody receptor staining. The

software was tuned to specifically locate and isolate the individualized pixel signals, then was

counted to provide an assessment of the number of receptors present. The distribution of the

pixels can also be visualized with the software to yield a sense of where the bulk of these

receptors tend to be located (Figure 34). A minority of slides had the appearance of either cutting

artifacts, from the cryotomy, or residual spots from the mounting medium and could result in

reducing the receptor distribution among the effected slides. However, since 10 slides or more

were used for each group, contribution of these errors on the accuracy of the distribution count

was considered low.
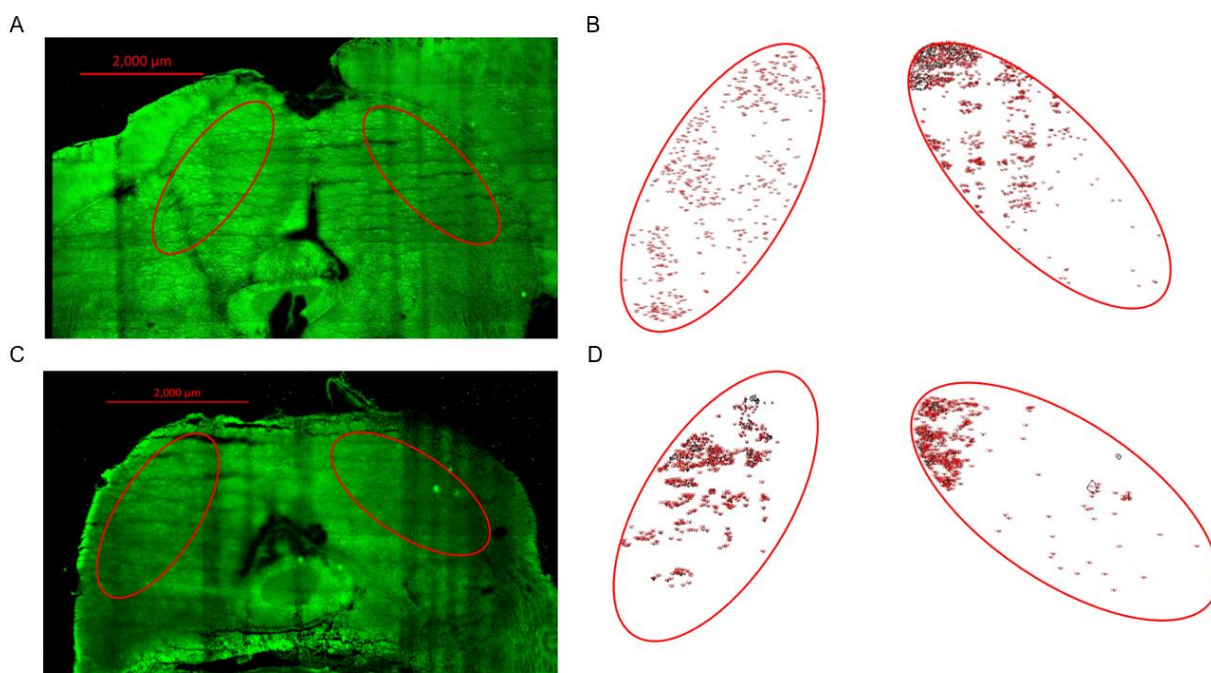
Figure 34. Comparison of ICC-stained brain section with corresponding positive receptor signals. (A) Sample image of control brain section. (B) Distribution of positive receptor staining in control subject. (C) Sample image of a noise exposed brain section. (D) Distribution of noise exposed subject receptors.

The aggregate of the positive signals was gathered under the software and could then be

comparatively examined with statistical analysis. All the stained slides were analyzed first

without regard to their stereotaxic coordinates and compared using an unpaired t-test to evaluate

receptor distribution across the control and noise exposed groups (Figure 35 A). The effect of

harmful noise was found to be statistically significant, $t(15) = 3.641$, p-value = 0.0024.

The slides were then segregated according to their associated stereotaxic coordinates for a more accurate account of the receptor distribution. The anatomic location is determined according to measurements taken by examining common landmarks on the rodent skull. The Bregma is a coronal suture across the skull and measures taken beyond this mark are designated as being positive Bregma, whereas measurements taken before this mark are defined as negative Bregma. A majority of the slides prepared fell into the -8.72 mm Bregma region and the comparative statistics were repeated (Figure 35 B). The resulting unpaired t-test also demonstrated statistical significance in the experimental groups, $t(11) = 4.000$, p-value $= 0.0021$.
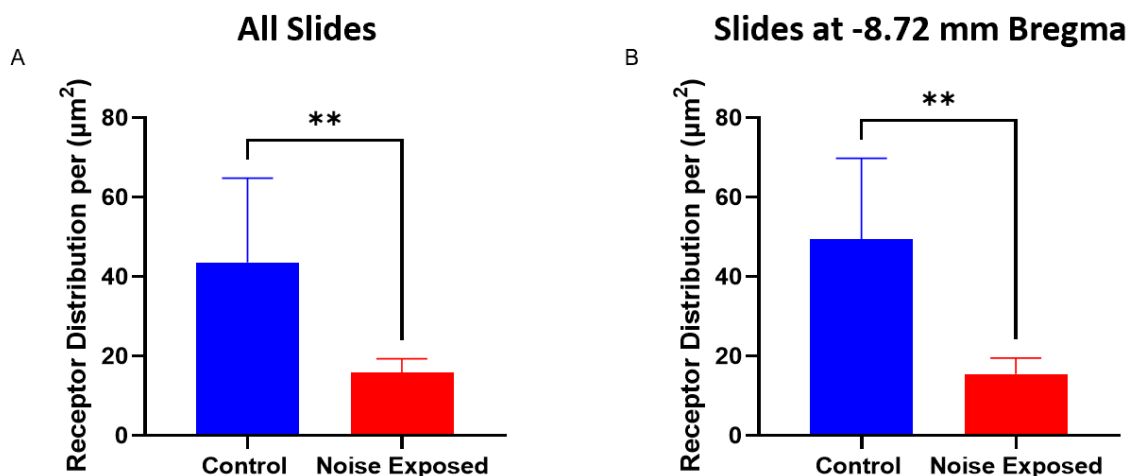
Figure 35. Comparison of D2 dopamine receptors distributed between control and noise exposed subjects. (A) Uncoordinated slide comparison found statistical significance according to an unpaired t-test, $t(15) = 3.641$, p-value $= 0.0024$. (B) Slide comparisons at -8.72 mm Bregma also found significant difference between experimental groups, $t(11) = 4.000$, p-value $= 0.0021$.

CHAPTER 5

DISCUSSION

The characterization of neurochemicals and their role in biological systems requires an approach that captures the complexity and elegance of neurotransmission. The focus of this study was to optimize an electroanalytical assay to characterize monoamines, such as dopamine, within the central auditory system in the rodent brain. The work also provided insight on the impact of loud noise on monoamine neurotransmission in the hub of central auditory responses and hinted on possible mechanistic options underlying the noise-induce effect.

5.1 Voltametric Assay to Characterize Dopamine Neurotransmission in the Inferior Colliculus

The operational effectiveness of any instrumental technique is contingent on its performance characteristics. Fast scan cyclic voltammetry (FSCV) is a sensitive and high temporal resolution analytical technique that has a wide application in biological systems. Like all other analytical methods, it was expedient to validate the FSCV assay to establish its fitness of purpose and to optimize the operational parameters before the slice measurements. The process also offers the opportunity to resolve possible analytical challenges that the complex biological environment may pose**.** FSCV was coupled with carbon fiber microelectrodes made in-house. The optimization and validation of the method included electrode conditioning and characterization using a flow-cell based FSCV system. Through continuously cycling the waveform potential at a higher frequency than the recording frequency, the surface of the carbon fiber was altered to improve the electrode's sensitivity. Once conditioned, the electrode demonstrated increased sensitivity towards electroactive analytes within the potential window of

the applied waveform. Each carbon fiber microelectrode was characterized to ensure that it maintained an optimal selectivity and sensitivity. Dopamine, being the chief analyte in this study, was used in the characterization and optimization of the operational parameters for the analytical system. The cyclic voltammogram generated provided a characteristic signature for the analyte and enabled it to be identified by means of the shape of the voltammogram and the location of the redox signals. Dopamine exhibited an oxidation peak at +0.6 V and a reduction peak at -0.2 V. Furthermore, developing a standard calibration curve established a relationship between the instrumental response (peak current) and the analyte concentration. The use of regression analysis provided sufficient evidence of a linear relationship between the analyte and the instrumental response. The regression analysis also allowed for other important figures of merit to be reported. Since monoamine neurotransmission in rodent models involves concentrations near the micro to nano molar ranges, it was expedient to demonstrate the ability of the analytical system to achieve limits of detection and quantification within or below this range. Our flow-cell based FSCV-microelectrode system indicated a limit of detection of 0.2 nM and a limit of quantification at 0.5 nM. Monoamine quantification technique, *in vivo* microdialysis paired with High Performance Liquid Chromatography (HPLC), has been reported to have a limit of detection of ~180 pM and limit of quantification ~1000 nM (M. Zhang et al., 2014). While the limit of detection is on the same order of magnitude as the current method, the limit of quantification of the latter is inferior to the former. Issues typically emerge when attempting to generate an adequate linear dynamic range for quantifying analytes at this low of a concentration due to the contribution from interferents that include metabolites in the monoamine pathway and other biomolecules. While derivatization reactions are typically used to improve the chromatography separation, the technique only provides quantitative measures of the

extracellular levels of the neurotransmitter rather than its release. FSCV on the other hand, has a

unique ability to measure neurotransmitter release and uptake on a millisecond time scale.

Additionally, the probe size used in the collection of monoamine samples in *in vivo*

microdialysis is large and disruptive often leading to tissue damage and immune response that

can confound the measurement (Chefer et al., 2009). FSCV maintains optimal detection and

quantification limits, while providing superior spatial resolution and biocompatibility due to the

use of smaller size carbon fiber microelectrodes. In FSCV, the selective nature of the waveform

also discriminates against the other electroactive species present, as they may not undergo redox

reactions within the same potential window selected (Gaweska & Fitzpatrick, 2011).

Ascorbic acid is a common antioxidant in the brain that can typically be an interferent in

electroanalytical measurements in biological environments. The ability of the method to

discriminate between the analyte (dopamine) and potential interferents, including ascorbic acid,

establishes the method's selectivity. The full potential window of ascorbic acid ranges from -1.0

to +0.8 V, which does have overlap with dopamine. The cyclic voltammogram, however,

displays a different oxidation peak potential, ~+5.5 V, and no reduction peak. The shape of the

voltammogram is markedly different, with a single oxidation peak appearing due to the

irreversible redox reaction occurring at the electrode surface. A comparison of the

voltammograms for dopamine and ascorbic acid provides a clear distinction in their identities.

Dopamine maintains a reduction peak at -0.2 V and an oxidation peak at +0.6 V. These features

provide a general foundation towards distinctively differentiating between these two analytes.

Regression analysis performed on the ascorbic acid calibration curve also confirmed the

calibration sensitivity of the method. Furthermore, the detection and quantification limits for the

ascorbic acid were 1.2 nM and 4.8 nM, respectively. The low limits of detection and

quantification for dopamine indicate the method's capabilities of being more sensitive towards the monoamine than ascorbic acid. Alternative ascorbic acid quantification methods, such as capillary electrophoresis and HPLC display limits of detection and quantification in the lower μM to high nM range (Gazdik et al., 2008; Wu et al., 2007). Both methods run into similar difficulties of sensitivity and selectivity.

Other optimization parameters of the considered was the scan rates of the waveform for each of the analytes. Each of the experiments did not find any better scan rate for the two analytes other than the previously established rate in the literature of 400 V/s and were not included as part of the optimized parameters of this study.

5.1.1 Voltammetry Implementation in Brain Slices

The complex chemical environment of biological tissues creates a wide range of potential detection and quantification challenges, requiring an analytical method capable of circumventing them. The strength of FSCV mentioned and demonstrated in the flow cell system make the method well positioned for brain measurements. FSCV measurements were made in brain slices. The advantage of performing FSCV on a brain slice is that the neural cell bodies have been mechanically detached from the terminal region in the brain slice, allowing for studies that are more focus on the dynamics at the axon terminal region. The influence from other brain regions becomes excluded leaving only the brain region of interest to be explored. Additionally, the application of pharmacological manipulations is much easier in brain slices than *in vivo* with minimal washout time required.

Using the parameters established by the flow cell calibrations, the electrodes were conditioned and pre-calibrated for slice measurements. Stimulation parameters employed were consistent with previous literature values (John & Jones, 2007). The delivery amperage could be

adjusted while attempting to establish a stable monoamine signal but was most often centered around 1 mA. Calibrated and conditioned electrodes ensures that optimization parameters of sensitivity and selective are maintained. Although the fabricated electrodes will inevitably have variations, they will also yield variable calibration factors that is essential towards making the conversion of the collected currents into concentration.

5.1.2 The Tale of Two Peaks

FSCV performed in the inferior colliculus of rat brain slices generated an unexpected presentation of two oxidation peaks and a single prominent reduction peak. While one of the oxidation peaks and the reduction peak had striking resemblance with the dopamine voltammogram, there appears to be a shift of these peaks from the expected potentials. Currently, much is not known about simultaneous detection of multiple biomolecules in the brain with FSCV. However, a shift in the oxidation and reduction peaks of a cyclic voltammogram is common, especially, when measurements are conducted in complex chemical environments. Adsorption of electrochemically inert materials may alter the presentation of expected peaks. The same as contributions from other interferants, such as pH and other charged ions like calcium (Takmakov et al., 2010). It is also possible that the appearance of these peaks is indicative of electrical artifacts. Despite these effects, the FSCV software can provide a multivariate calibration through the construction of training sets as applied through principal component regression analysis to determine analyte concentration (Keithley & Wightman, 2011). In addition, Fourier transformations are available in the FSCV instrumental software package as a means towards filtering and smoothing the data (Bucher et al., 2013). The effect of this filtering allowed for the isolation of one of the oxidation peaks which further reflected a change in the shape of the cyclic voltammogram, appearing more aligned with the typical dopamine

signature. The voltammogram combined with the training set analysis provided the first degrees of evidence that suggest dopamine was being recorded in the inferior colliculus. To confirm this assertion, the brain slices were pharmacologically manipulated to examine the impact on the analytical signal.

Pharmacological manipulations are a common addition to FSCV analysis and are integral in identifying, confirming, and characterizing a detected analyte (Brodnik et al., 2020). First the brain slices were challenged with tetrabenazine, a drug that inhibits vesicular monoamine transporter 2 (VMAT 2). This transporter packages monoamines, such as dopamine and norepinephrine, into vesicles upon synthesis and are stored until they are released during neurotransmission. The perfusion of tetrabenazine demonstrated concentration-dependent attenuation in signals for the two oxidation peaks, suggesting them to be signals from monoamines. Further pharmacological studies with drugs that are selective for dopamine receptors, such as quinpirole (D2 receptor agonist), sulpiride (D2 receptor antagonist) and 7-OH-DPAT (D3 receptor agonist), also yielded a dose-dependent decrease in the peak 1 signal, but not much alteration in the peak 2 signal. These data provided sufficient evidence to conclude the identity of peak 1 to be dopamine, an inference that is consistent with the Fourier transformations. The data also implicates norepinephrine as a possible candidate responsible for peak 2. Norepinephrine is a well-known monoamine neurotransmitter synthesized from dopamine by dopamine β-hydroxylase. Existing data have demonstrated the presence of this monoamine in the inferior colliculus by HPLC (Browning et al., 1991). Additionally, the inferior colliculus has also been shown to contain noradrenergic receptors (Klepper & Herbert, 1991), suggesting that norepinephrine plays a role in auditory processing.

5.2 Characterizing the Effect of Loud Noise on
Monoamine Neurotransmission

Exposure to loud noise can cause deafness and other hearing disorders, including tinnitus. While existing work has demonstrated that deafening noise elicits changes in spontaneous neuronal activity in key auditory brain regions, including the inferior colliculus, the exact neural substrate is not known. As dopamine is now implicated in the auditory process, we examine how loud noise impacts on its transmission in the hub of auditory processes. The present data revealed significant reduction in dopamine release 24-hours following noise exposure., implicating dopamine neurotransmission in noise-induced deafness related changes in the inferior colliculus. Sex differences have the potential to influence a variety of chemicals throughout the body and were considered a possible variation in this study. However, the analysis of the subjects separated by sex ultimately found that no inherent difference was present (see Appendix A). The effect of noise appears to be long-lasting, as changes in dopamine release persisted three days after noise exposure.

The appearance of both oxidation peaks remained present in the sound exposed subjects. Pre-calibration training sets were developed for dopamine, as previously outlined in section 5.1.1., and the current signals were converted into concentration. Since norepinephrine was not originally expected, a single pre-calibrated training set established for the control subjects was extended for use in the noise exposed subjects to retain the consistency of the current to concentration conversion. Filtering of the data was also consistent for the noise exposed subjects as it had for the control subjects, effectively verifying the continued presence of both monoamines after exposure to harmful noise. The effects of the noise exposure displayed clearly depressed signals in both monoamines. The extent of the decrease in the release of these

monoamines elicited by the noise exposure provides evidence of the connection that they have in hearing.

5.3 Plausible Mechanism for Deafness Related
Changes in Monoamine Neurotransmission

Due to the noise-induced decreased in dopamine release, we hypothesized this effect could be elicit via the feedback inhibition loop. The mechanism occurs through three primary stages. First, inhibitory dopamine autoreceptors decrease vesicular release through activation of calcium channels which lowers the amount of calcium entering the neuron. Next, autoreceptors also increase the activity of plasma membrane proteins, which increase the rate of reuptake back into the neuron, decreasing the concentration of dopamine within the neural synaptic space. Finally, any long term activation of the autoreceptors results in a decrease in activation of tyrosine hydroxylase, which ultimately results in a further decrease in the synthesis and packaging of monoamines in the neuron's vesicles (Ford, 2014). To verify the present hypothesis, the effect of noise on three main targets within the feedback inhibition loop was examined, namely the D2 autoreceptors, dopamine synthesis, and packaging into vesicles.

Modulation of dopamine receptor genes in auditory processing following acoustic damage in the inferior colliculus has been reported by previous work (Gittelman et al., 2013b), yet a direct comparison of D2 receptors in noise exposed subjects has not been previously characterized. The D2 autoreceptors functionality was examined using FSCV and pharmacology. Changes to the dopamine autoreceptor (D2 and D3) inhibitory action would support the feedback inhibition as a plausible mechanism of the effect of noise. Repeats of the drugs selective for dopamine receptors; quinpirole, sulpiride, and 7-OH-DPAT yielded a similar response to the control studies. Statistical analysis comparing the control and noise exposed groups found there was no significant difference in the response to the drugs. This data provides enough evidence to

conclude that noise did not impact dopamine autoreceptor (D2 and D3) functionality directly.

The possible impact of noise on dopamine receptors was further explored by comparing their

distribution after the noise exposed. Immunocytochemistry was used to accomplish this goal.

Immunocytochemistry allows for the distribution of the receptors in the region of interest to be

studied. Comparisons of the distribution of positive receptor staining in the inferior colliculus

showed a greater density near the central nucleus. A major processing and integration center of

auditory information, the central nucleus of the inferior colliculus receives input from the

ascending auditory pathway (Goyer et al., 2019). The significant difference presented between

the control and noise exposed subjects suggests that noise exposure alters D2 receptor

distribution in the inferior colliculus. A difference in the distribution of the autoreceptors

challenges the feedback inhibition loop hypothesis, since the number of receptors were reduced,

and the functionality was not altered. This suggests that the damage from noise is more

widespread and multifaceted.

The large reduction in monoamine release further implicates the impacts of noise on

monoamine synthesis and packaging as both neurotransmitters are linked through this pathway

and both were affected. Alpha-methyl-p-tyrosine (AMPT) operates by inhibiting tyrosine

hydroxylase, the rate-determining enzyme in monoamine synthesis. This was combined with

tetrabenazine, which inhibits vesicular transport to the synapse, to further study the depletion of

monoamine release. The drug perfusion followed suit with the control experiments generating a

drug response curve that displayed a steeper slope than tetrabenazine alone, representing the

extent to which the inhibition had taken place. Modulation to the synthesis and vesicular

packaging produced similar levels of inhibition to both dopamine and norepinephrine, suggesting

the effects of the noise damage are likely coming from something not directly linked to the

synthesis and packaging pathway. Existing evidence may implicate oxidative stress as a potential mechanism underlying the effect of noise the monoamine release. Oxidative stress involves excessive production of reactive oxygen species that emerged from the chemical stress being imposed on the nervous system during periods of exposure to harmful levels of noise.

5.4 Conclusions and Recommendations
for Future Study

The primary aim of this research was to assess the impacts of harmful noise on monoamine neurotransmission in the hub of central auditory responses. To accomplish this task, there was the need to identify and optimize an analytical method to detect and monitor monoamine release. Next, the technique was utilized to compare monoamine transmission between control versus noise exposed groups. Finally, the potential underlying mechanisms behind the effect of noise was explored.

5.4.1 Conclusions from
Objective 1

Fast scan cyclic voltammetry was selected as an appropriate method to characterize electroactive monoamines in the brain due to its speed, sensitivity, selectivity, and its ability to utilize microelectrodes to make measurements from sub-anatomical brain regions. The complex biological and chemical makeup of the brain required optimization of the FSCV assay using flow-cell analysis. The optimized parameters established in the flow-cell calibration and characterization were incorporated in the slice monoamine measurements. Two oxidation peaks in the cyclic voltammograms were detected and identified to be dopamine and norepinephrine, using FSCV and pharmacological manipulations. Thus, this work reports simultaneous detection of these monoamines in the inferior colliculus.

5.4.2 Conclusions from Objective 2

FSCV measurements were made from the inferior colliculus of rats that were exposed to harmful levels of noise to invoke deafness. The presence of both oxidation peaks remained following noise exposure. Concentrations of both dopamine and norepinephrine released were found to be significantly reduced in the noise exposed groups compared to their controls. This effect of noise on dopamine neurotransmission was demonstrated to be long-lasting. Confirmation of both analytes were assessed with training sets established using the analysis software's principal component regression capabilities.

5.4.3 Conclusions from Objective 3

The feedback loop mechanism was tested as a means towards explaining the reduction in neurotransmitter release following exposure to harmful noise and tested through analysis of dopamine autoreceptors, dopamine synthesis, and vesicular packaging. The distribution of receptors was found to be significantly different among experimental groups. Pharmacological manipulation of receptor functionality was also not significantly impacted. Further modification of the synthesis pathway with pharmacological agents displayed no significant impact in the effectiveness of the neurons to package or synthesize monoamines. The impact of noise on the concentration of monoamine release must be resulting from another source, possibly through oxidative stress mechanism.

5.4.4 Overall Conclusions

The present work presented FSCV utility in flow-cell and in brain slices. The method demonstrated high sensitivity, selectivity, and limits of detection and quantification. The

application of the method in brain slices allowed simultaneous measurement of monoamines whose identities were verified to be dopamine and possibly, norepinephrine used with pharmacological studies. This work also demonstrated for the first time that deafening noise downregulates monoamine neurotransmission in the inferior colliculus, an effect that was proven to be long-term. While this noise-induced effect in the hub of auditory responses did not appear to involve direct alteration in VMAT 2 and dopamine autoreceptor function; the distribution did present a significant difference among experimental groups. The role of the feedback inhibition loop is less likely, and the effects of damaging noise are more widespread throughout the brain.

5.5 Future Directions

Detection of multiple electroactive analytes by FSCV simultaneously has not been previously reported. The early findings in this study open the door to many other applications that may extend beyond a biological system. Limitations in the instrumental software made it difficult to isolate the signals from one another and could be improved upon to enhance selectivity between the two monoamines in slice measurements. Furthermore, instrumental innovations to FSCV could employ electrode modifications to delineate between the dual detection of analytes.

The identification of dopamine and norepinephrine in the inferior colliculus implicates both monoamines in central auditory processes. Norepinephrine was suspected as a co-detected analyte through the process of exclusion and the effects of dopamine-related pharmacology. More pharmacological studies should be employed at specifically targeting norepinephrine and related receptors in the inferior colliculus. Further studies should also expand the exact roles of these neurotransmitters on the central pathway and their possible connections to the peripheral auditory systems. The extent and role to which these monoamines operate may also provide

clinicians with a route towards developing effective therapeutic interventions for hearing-related disorders, including hearing loss and tinnitus.

The role of dopamine in auditory processing remains an open field for investigation. This study can extend into behavioral and learning effects of hearing. An overall distribution of the D2-like receptors in the inferior colliculus was changed, the impact of noise on the feedback inhibition mechanism may still be tested further. Few options are possible towards explaining the mechanism underlying the noise-induced attenuation in monoamine transmission, including oxidative stress that should also be explored. These new steps may shed more light on the role monoamines play in auditory neural signaling.

REFERENCES

Abdalla, A., Atcherley, C. W., Pathirathna, P., Samaranayake, S., Qiang, B., Peña, E., Morgan, S. L., Heien, M. L., & Hashemi, P. (2017). In Vivo Ambient Serotonin Measurements at Carbon-Fiber Microelectrodes. *Analytical Chemistry*, *89*(18), 9703–9711. https://doi.org/10.1021/acs.analchem.7b01257

Basta, D., & Ernest, A. (2004). Noise-induced changes of neuronal spontaneous activity in mice inferior colliculus brain slices. *Neuroscience Letters*, *368*(3), 297–302. https://doi.org/10.1016/j.neulet.2004.07.030

Batton, A. D., Blaha, C. D., Bieber, A., Lee, K. H., & Boschen, S. L. (2019). Stimulation of the subparafascicular thalamic nucleus modulates dopamine release in the inferior colliculus of rats. *Synapse*, *73*(2), e22073. https://doi.org/10.1002/syn.22073

Brodnik, Z. D., Xu, W., Batra, A., Lewandowski, S. I., Ruiz, C. M., Mortensen, O. V., Kortagere, S., Mahler, S. V., & España, R. A. (2020). Chemogenetic Manipulation of Dopamine Neurons Dictates Cocaine Potency at Distal Dopamine Transporters. *Journal of Neuroscience*, *40*(45), 8767–8779. https://doi.org/10.1523/JNEUROSCI.0894-20.2020

Brogden, R. N., Heel, R. C., Speight, T. M., & Avery, G. S. (1981). alpha-Methyl-p-tyrosine: A review of its pharmacology and clinical use. *Drugs*, *21*(2), 81–89. https://doi.org/10.2165/00003495-198121020-00001

Browning, R. A., Wang, C., & Faingold, C. L. (1991). Effect of norepinephrine depletion on audiogenic-like seizures elicited by microinfusion of an excitant amino acid into the

inferior colliculus of normal rats. *Experimental Neurology*, *112*(2), 200–205. https://doi.org/10.1016/0014-4886(91)90070-S

Bucher, E. S., Brooks, K., Verber, M. D., Keithley, R. B., Owesson-White, C., Carroll, S., Takmakov, P., McKinney, C. J., & Wightman, R. M. (2013). Flexible Software Platform for Fast-Scan Cyclic Voltammetry Data Acquisition and Analysis. *Analytical Chemistry*, *85*(21), 10344–10353. https://doi.org/10.1021/ac402263x

Caley, C. F., & Weber, S. S. (1995). Sulpiride: An antipsychotic with selective dopaminergic antagonist properties. *The Annals of Pharmacotherapy*, *29*(2), 152–160. https://doi.org/10.1177/106002809502900210

Carroll, Y. I. (2017). Vital Signs: Noise-Induced Hearing Loss Among Adults — United States 2011–2012. *MMWR. Morbidity and Mortality Weekly Report*, *66*. https://doi.org/10.15585/mmwr.mm6605e3

Chefer, V. I., Thompson, A. C., Zapata, A., & Shippenberg, T. S. (2009). Overview of Brain Microdialysis. *Current Protocols in Neuroscience / Editorial Board, Jacqueline N. Crawley ... [et Al.]*, *CHAPTER*, Unit7.1. https://doi.org/10.1002/0471142301.ns0701s47

Chen, G.-D., Sheppard, A., & Salvi, R. (2016). Noise trauma induced plastic changes in brain regions outside the classical auditory pathway. *Neuroscience*, *315*, 228–245. https://doi.org/10.1016/j.neuroscience.2015.12.005

Chu, E., Chu, J., Socci, R. R., & Chu, T.-C. (2004). 7-OH-DPAT-induced inhibition of norepinephrine release in PC12 cells. *Pharmacology*, *70*(3), 130–139. https://doi.org/10.1159/000074976

Cope, T. E., Baguley, D. M., & Griffiths, T. D. (2015). The functional anatomy of central auditory processing. *Practical Neurology*, *15*(4), 302–308. https://doi.org/10.1136/practneurol-2014-001073

Eagle, D. M., Noschang, C., d'Angelo, L.-S. C., Noble, C. A., Day, J. O., Dongelmans, M. L., Theobald, D. E., Mar, A. C., Urcelay, G. P., Morein-Zamir, S., & Robbins, T. W. (2014). The dopamine D2/D3 receptor agonist quinpirole increases checking-like behaviour in an operant observing response task with uncertain reinforcement: A novel possible model of OCD. *Behavioural Brain Research*, *264*(100), 207–229. https://doi.org/10.1016/j.bbr.2013.12.040

Ferraro, S., Nanetti, L., Piacentini, S., Mandelli, M. L., Bertolino, N., Ghielmetti, F., Epifani, F., Nigri, A., Taroni, F., Bruzzone, M. G., Donato, S. D., Savoiardo, M., Mariotti, C., & Grisoli, M. (2014). Frontal cortex BOLD signal changes in premanifest Huntington disease: A possible fMRI biomarker. *Neurology*, *83*(1), 65–72. https://doi.org/10.1212/WNL.0000000000000538

Folmer, R. L., Vachhani, J. J., Theodoroff, S. M., Ellinger, R., & Riggins, A. (2017). *Auditory Processing Abilities of Parkinson's Disease Patients* [Research article]. BioMed Research International. https://doi.org/10.1155/2017/2618587

Ford, C. P. (2014). The Role of D2-Autoreceptors in Regulating Dopamine Neuron Activity and Transmission. *Neuroscience*, *282*, 13–22. https://doi.org/10.1016/j.neuroscience.2014.01.025

Fyk-Kolodziej, B. E., Shimano, T., Gafoor, D., Mirza, N., Griffith, R. D., Gong, T.-W., & Holt, A. G. (2015). Dopamine in the auditory brainstem and midbrain: Co-localization with

amino acid neurotransmitters and gene expression following cochlear trauma. *Frontiers in Neuroanatomy*, *9*. https://doi.org/10.3389/fnana.2015.00088

Gaweska, H., & Fitzpatrick, P. F. (2011). Structures and Mechanism of the Monoamine Oxidase Family. *Biomolecular Concepts*, *2*(5), 365–377. https://doi.org/10.1515/BMC.2011.030

Gazdik, Z., Zitka, O., Petrlova, J., Adam, V., Zehnalek, J., Horna, A., Reznicek, V., Beklova, M., & Kizek, R. (2008). Determination of Vitamin C (Ascorbic Acid) Using High Performance Liquid Chromatography Coupled with Electrochemical Detection. *Sensors (Basel, Switzerland)*, *8*(11), 7097–7112. https://doi.org/10.3390/s8117097

Gittelman, J. X., Perkel, D. J., & Portfors, C. V. (2013a). Dopamine Modulates Auditory Responses in the Inferior Colliculus in a Heterogeneous Manner. *JARO: Journal of the Association for Research in Otolaryngology*, *14*(5), 719–729. https://doi.org/10.1007/s10162-013-0405-0

Gittelman, J. X., Perkel, D. J., & Portfors, C. V. (2013b). Dopamine Modulates Auditory Responses in the Inferior Colliculus in a Heterogeneous Manner. *Journal of the Association for Research in Otolaryngology*, *14*(5), 719–729. https://doi.org/10.1007/s10162-013-0405-0

Goyer, D., Silveira, M. A., George, A. P., Beebe, N. L., Edelbrock, R. M., Malinski, P. T., Schofield, B. R., & Roberts, M. T. (2019). A novel class of inferior colliculus principal neurons labeled in vasoactive intestinal peptide-Cre mice. *ELife*, *8*, e43770. https://doi.org/10.7554/eLife.43770

Gu, H., Varner, E. L., Groskreutz, S. R., Michael, A. C., & Weber, S. G. (2015). In Vivo Monitoring of Dopamine by Microdialysis with 1 min Temporal Resolution Using Online

Capillary Liquid Chromatography with Electrochemical Detection. *Analytical Chemistry*, *87*(12), 6088–6094. https://doi.org/10.1021/acs.analchem.5b00633

Guru, A., Post, R. J., Ho, Y.-Y., & Warden, M. R. (2015). Making Sense of Optogenetics. *International Journal of Neuropsychopharmacology*, *18*(11). https://doi.org/10.1093/ijnp/pyv079

Hermans, A., Seipel, A. T., Miller, C. E., & Wightman, R. M. (2006). Carbon-fiber microelectrodes modified with 4-sulfobenzene have increased sensitivity and selectivity for catecholamines. *Langmuir: The ACS Journal of Surfaces and Colloids*, *22*(5), 1964–1969. https://doi.org/10.1021/la053032e

Holt, A. G., Asako, M., Lomax, C. A., MacDonald, J. W., Tong, L., Lomax, M. I., & Altschuler, R. A. (2005a). Deafness-related plasticity in the inferior colliculus: Gene expression profiling following removal of peripheral activity. *Journal of Neurochemistry*, *93*(5), 1069–1086. https://doi.org/10.1111/j.1471-4159.2005.03090.x

Holt, A. G., Asako, M., Lomax, C. A., MacDonald, J. W., Tong, L., Lomax, M. I., & Altschuler, R. A. (2005b). Deafness-related plasticity in the inferior colliculus: Gene expression profiling following removal of peripheral activity. *Journal of Neurochemistry*, *93*(5), 1069–1086. https://doi.org/10.1111/j.1471-4159.2005.03090.x

Huddle, M. G., Goman, A. M., Kernizan, F. C., Foley, D. M., Price, C., Frick, K. D., & Lin, F. R. (2017). The Economic Impact of Adult Hearing Loss: A Systematic Review. *JAMA Otolaryngology–Head & Neck Surgery*, *143*(10), 1040–1048. https://doi.org/10.1001/jamaoto.2017.1243

Jaber, M., Robinson, S. W., Missale, C., & Caron, M. G. (1996). Dopamine receptors and brain function. *Neuropharmacology*, *35*(11), 1503–1519.

Jang, D. P., Kim, I., Chang, S.-Y., Min, H. K., Arora, K., Marsh, M. P., Hwang, S.-C., Kimble, C. J., Bennet, K. E., & Lee, K. H. (2012). Paired Pulse Voltammetry for differentiating complex analytes. *The Analyst*, *137*(6), 1428–1435. https://doi.org/10.1039/c2an15912k

John, C. E., & Jones, S. R. (2007). Fast Scan Cyclic Voltammetry of Dopamine and Serotonin in Mouse Brain Slices. In A. C. Michael & L. M. Borland (Eds.), *Electrochemical Methods for Neuroscience*. CRC Press/Taylor & Francis. http://www.ncbi.nlm.nih.gov/books/NBK2579/

Keithley, R. B., & Wightman, R. M. (2011). Assessing Principal Component Regression Prediction of Neurochemicals Detected with Fast-Scan Cyclic Voltammetry. *ACS Chemical Neuroscience*, *2*(9), 514–525. https://doi.org/10.1021/cn200035u

Klepper, A., & Herbert, H. (1991). Distribution and origin of noradrenergic and serotonergic fibers in the cochlear nucleus and inferior colliculus of the rat. *Brain Research*, *557*(1), 190–201. https://doi.org/10.1016/0006-8993(91)90134-H

Lai, S.-W., Liao, K.-F., Lin, C.-L., Lin, C.-C., & Sung, F.-C. (2014). Hearing loss may be a non-motor feature of Parkinson's disease in older people in Taiwan. *European Journal of Neurology*, *21*(5), 752–757. https://doi.org/10.1111/ene.12378

Lama, R. D., Charlson, K., Anantharam, A., & Hashemi, P. (2012). Ultrafast Detection and Quantification of Brain Signaling Molecules with Carbon Fiber Microelectrodes. *Analytical Chemistry*, *84*(19), 8096–8101. https://doi.org/10.1021/ac301670h

Lemaître, F., Guille Collignon, M., & Amatore, C. (2014). Recent advances in Electrochemical Detection of Exocytosis. *Electrochimica Acta*, *140*, 457–466. https://doi.org/10.1016/j.electacta.2014.02.059

Levey, A. I., Hersch, S. M., Rye, D. B., Sunahara, R. K., Niznik, H. B., Kitt, C. A., Price, D. L., Maggio, R., Brann, M. R., & Ciliax, B. J. (1993). Localization of D1 and D2 dopamine receptors in brain with subtype-specific antibodies. *Proceedings of the National Academy of Sciences*, *90*(19), 8861–8865. https://doi.org/10.1073/pnas.90.19.8861

Lin, F. R., Niparko, J. K., & Ferrucci, L. (2011). Hearing Loss Prevalence in the United States. *Archives of Internal Medicine*, *171*(20), 1851–1853. https://doi.org/10.1001/archinternmed.2011.506

Lin, M. Z., & Schnitzer, M. J. (2016). Genetically encoded indicators of neuronal activity. *Nature Neuroscience*, *19*(9), 1142–1153. https://doi.org/10.1038/nn.4359

Maina, F. K., Khalid, M., Apawu, A. K., & Mathews, T. A. (2012). Presynaptic dopamine dynamics in striatal brain slices with fast-scan cyclic voltammetry. *Journal of Visualized Experiments: JoVE*, *59*. https://doi.org/10.3791/3464

Middleton, J. W., & Tzounopoulos, T. (2012). Imaging the neural correlates of tinnitus: A comparison between animal models and human studies. *Frontiers in Systems Neuroscience*, *6*. https://doi.org/10.3389/fnsys.2012.00035

Mize, R. R., Holdefer, R. N., & Nabors, L. B. (1988). Quantitative immunocytochemistry using an image analyzer. I. Hardware evaluation, image processing, and data analysis. *Journal of Neuroscience Methods*, *26*(1), 1–23. https://doi.org/10.1016/0165-0270(88)90125-2

Moussaron, A., Vibhute, S., Bianchi, A., Gündüz, S., Kotb, S., Sancey, L., Motto-Ros, V., Rizzitelli, S., Crémillieux, Y., Lux, F., Logothetis, N. K., Tillement, O., & Angelovski, G. (2015). Ultrasmall Nanoplatforms as Calcium-Responsive Contrast Agents for Magnetic Resonance Imaging. *Small*, *11*(37), 4900–4909. https://doi.org/10.1002/smll.201500312

Nabors, L. B., Songu-Mize, E., & Mize, R. R. (1988). Quantitative immunocytochemistry using an image analyzer. II. Concentration standards for transmitter immunocytochemistry. *Journal of Neuroscience Methods*, *26*(1), 25–34. https://doi.org/10.1016/0165-0270(88)90126-4

Nevue, A. A., Elde, C. J., Perkel, D. J., & Portfors, C. V. (2016). Dopaminergic Input to the Inferior Colliculus in Mice. *Frontiers in Neuroanatomy*, *9*. https://doi.org/10.3389/fnana.2015.00168

Oh, Y., Kim, D. H., Shin, H., Park, C., Chang, S.-Y., Blaha, C. D., Bennet, K. E., Kim, I. Y., Lee, K. H., & Jang, D. P. (2015). Optimization of Paired Pulse Voltammetry Using Sawhorse Waveform. *Int. J. Electrochem. Sci.*, *10*, 13.

Paxinos, G., & Watson, C. (2013). *The Rat Brain in Stereotaxic Coordinates*. Academic Press.

Peterson, D. C., & Hamel, R. N. (2019). Neuroanatomy, Auditory Pathway. In *StatPearls*. StatPearls Publishing. http://www.ncbi.nlm.nih.gov/books/NBK532311/

Roberts, J. G., & Sombers, L. A. (2018). Fast Scan Cyclic Voltammetry: Chemical Sensing in the Brain and Beyond. *Analytical Chemistry*, *90*(1), 490–504. https://doi.org/10.1021/acs.analchem.7b04732

Robinson, D. L., Venton, B. J., Heien, M. L. A. V., & Wightman, R. M. (2003). Detecting subsecond dopamine release with fast-scan cyclic voltammetry in vivo. *Clinical Chemistry*, *49*(10), 1763–1773.

Rodeberg, N. T., Sandberg, S. G., Johnson, J. A., Phillips, P. E. M., & Wightman, R. M. (2017). Hitchhiker's Guide to Voltammetry: Acute and Chronic Electrodes for in Vivo Fast-Scan Cyclic Voltammetry. *ACS Chemical Neuroscience*, *8*(2), 221–234. https://doi.org/10.1021/acschemneuro.6b00393

Schou-Pedersen, A. M. V., Hansen, S. N., Tveden-Nyborg, P., & Lykkesfeldt, J. (2016).
Simultaneous quantification of monoamine neurotransmitters and their biogenic
metabolites intracellularly and extracellularly in primary neuronal cell cultures and in
sub-regions of guinea pig brain. *Journal of Chromatography B*, *1028*, 222–230.
https://doi.org/10.1016/j.jchromb.2016.05.048

Shaheen, L. A., & Liberman, M. C. (2018). Cochlear Synaptopathy Changes Sound-Evoked
Activity Without Changing Spontaneous Discharge in the Mouse Inferior Colliculus.
Frontiers in Systems Neuroscience, *12*. https://doi.org/10.3389/fnsys.2018.00059

Speck, I., Arndt, S., Thurow, J., Blazhenets, G., Aschendorff, A., Meyer, P. T., & Frings, L.
(2020). 18F-FDG PET Imaging of the Inferior Colliculus in Asymmetric Hearing Loss.
Journal of Nuclear Medicine, *61*(3), 418–422.
https://doi.org/10.2967/jnumed.119.231407

Takmakov, P., Zachek, M. K., Keithley, R. B., Bucher, E. S., McCarty, G. S., & Wightman, R.
M. (2010). Characterization of Local pH Changes in Brain Using Fast-Scan Cyclic
Voltammetry with Carbon Microelectrodes. *Analytical Chemistry*, *82*(23), 9892–9900.
https://doi.org/10.1021/ac102399n

Taylor, S. C., & Posch, A. (2014). *The Design of a Quantitative Western Blot Experiment*
[Research article]. BioMed Research International. https://doi.org/10.1155/2014/361590

Tong, L., Altschuler, R. A., & Holt, A. G. (2005). Tyrosine hydroxylase in rat auditory midbrain:
Distribution and changes following deafness. *Hearing Research*, *206*(1–2), 28–41.
https://doi.org/10.1016/j.heares.2005.03.006

Tuominen, L., Nummenmaa, L., Keltikangas-Järvinen, L., Raitakari, O., & Hietala, J. (2014). Mapping neurotransmitter networks with PET: An example on serotonin and opioid systems. *Human Brain Mapping*, *35*(5), 1875–1884. https://doi.org/10.1002/hbm.22298

Wang, Q., & Li, L. (2018). Differences between auditory frequency-following responses and onset responses: Intracranial evidence from rat inferior colliculus. *Hearing Research*, *357*, 25–32. https://doi.org/10.1016/j.heares.2017.10.014

Webster, J. G. (2009). *Medical Instrumentation Application and Design*. John Wiley & Sons.

Wu, T., Guan, Y., & Ye, J. (2007). Determination of flavonoids and ascorbic acid in grapefruit peel and juice by capillary electrophoresis with electrochemical detection. *Food Chemistry*, *100*(4), 1573–1579. https://doi.org/10.1016/j.foodchem.2005.12.042

Yang, C., Jacobs, C. B., Nguyen, M. D., Ganesana, M., Zestos, A. G., Ivanov, I. N., Puretzky, A. A., Rouleau, C. M., Geohegan, D. B., & Venton, B. J. (2016). Carbon Nanotubes Grown on Metal Microelectrodes for the Detection of Dopamine. *Analytical Chemistry*, *88*(1), 645–652. https://doi.org/10.1021/acs.analchem.5b01257

Yang, H., Thompson, A. B., McIntosh, B. J., Altieri, S. C., & Andrews, A. M. (2013). Physiologically Relevant Changes in Serotonin Resolved by Fast Microdialysis. *ACS Chemical Neuroscience*, *4*(5), 790–798. https://doi.org/10.1021/cn400072f

Yankaskas, K. (2013). Prelude: Noise-induced tinnitus and hearing loss in the military. *Hearing Research*, *295*, 3–8. https://doi.org/10.1016/j.heares.2012.04.016

Yero, T., & Rey, J. A. (2008). Tetrabenazine (Xenazine), An FDA-Approved Treatment Option For Huntington's Disease–Related Chorea. *Pharmacy and Therapeutics*, *33*(12), 690–694.

Zhang, J. S., & Kaltenbach, J. A. (1998). Increases in spontaneous activity in the dorsal cochlear nucleus of the rat following exposure to high-intensity sound. *Neuroscience Letters*, *250*(3), 197–200. https://doi.org/10.1016/S0304-3940(98)00482-0

Zhang, M., Fang, C., & Smagin, G. (2014). Derivatization for the simultaneous LC/MS quantification of multiple neurotransmitters in extracellular fluid from rat brain microdialysis. *Journal of Pharmaceutical and Biomedical Analysis*, *100*, 357–364. https://doi.org/10.1016/j.jpba.2014.08.015

APPENDIX A

**MONOAMINE COMPARISON IN THE
INFERIOR COLLICULUS
BY GENDER**
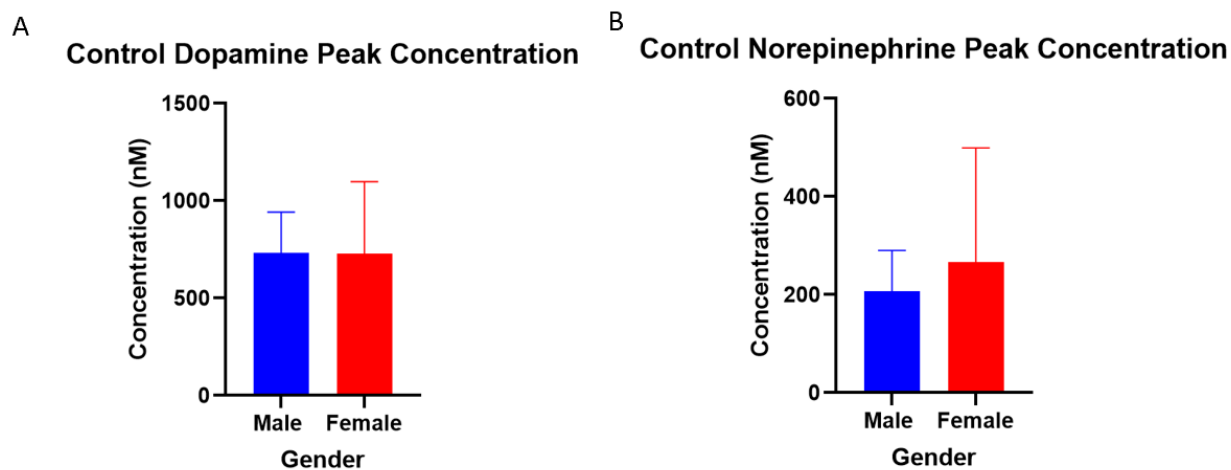
Figure 36. Comparison of gender on monoamine release in the inferior colliculus. (A) Dopamine release by gender displayed no statistically significant difference, $t(8) = 0.5576$, p-value = 0.5924. (B) Norepinephrine release by gender found no statistically significant difference, $t(8) = 0.5366$, p-value = 0.6061.

APPENDIX B

**PHARMACOLOGICAL CONCENTRATION VS TIME
TRACES OF NOISE EXPOSED SUBJECTS**
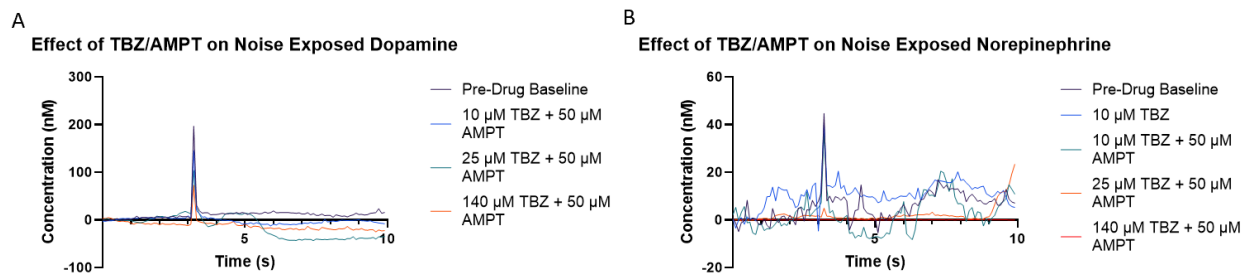
Figure 37. Noise exposed brain slice perfused with TBZ and AMPT cocktail. (A) Effect of drug cocktail on dopamine neurotransmission yields decreased peak concentration release with increasing drug concentration perfusion. (B) Impacts of the combination drug cocktail on norepinephrine neurotransmission indicating decreased peak concentration release related with increasing drug concentration perfusion.
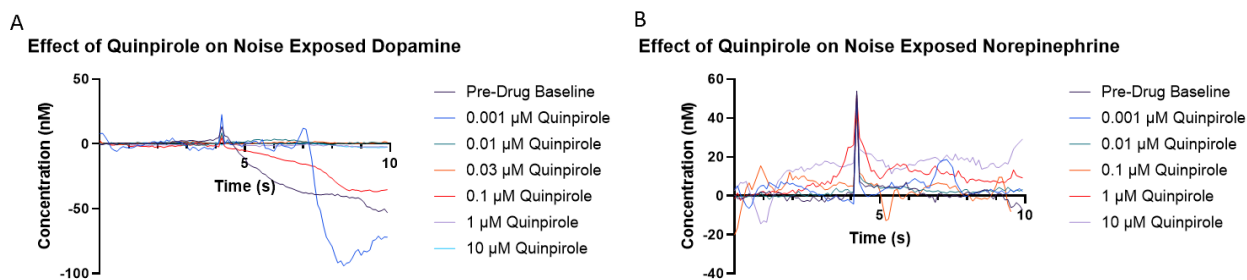

Figure 38. Effect of quinpirole on noise exposed subject group. (A) Dopamine peak concentration decreases with increasing drug concentration. (B) Norepinephrine peak concentration remains consistent with changing drug concentration.
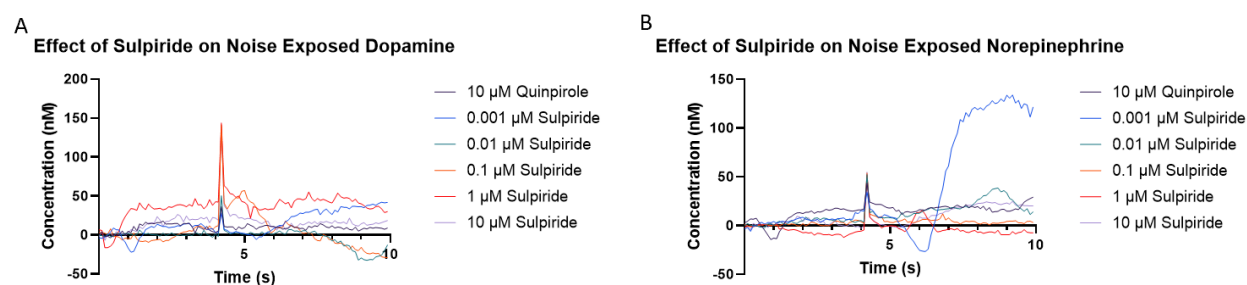

Figure 39. Effect of sulpiride on noise exposed subject group following quinpirole perfusion. (A) Dopamine peak concentration increases with increasing drug concentration. (B) Norepinephrine peak concentration is maintained with changing drug concentration.
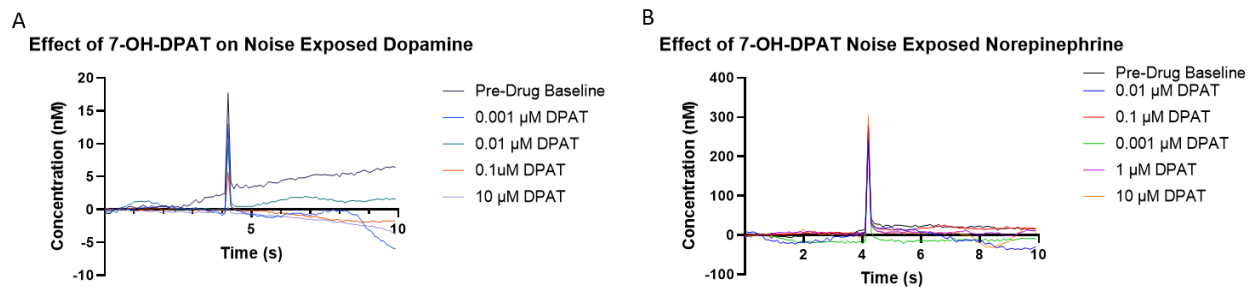
Figure 40. Effect of 7-OH-DPAT drug perfusion on noise exposed subject monoamine peak release concentration. (A) Peak dopamine release concentration decreases with increasing drug concentration. (B) Peak norepinephrine concentration stays consistent with changes in 7-OH-DPAT perfusion concentration.

APPENDIX C
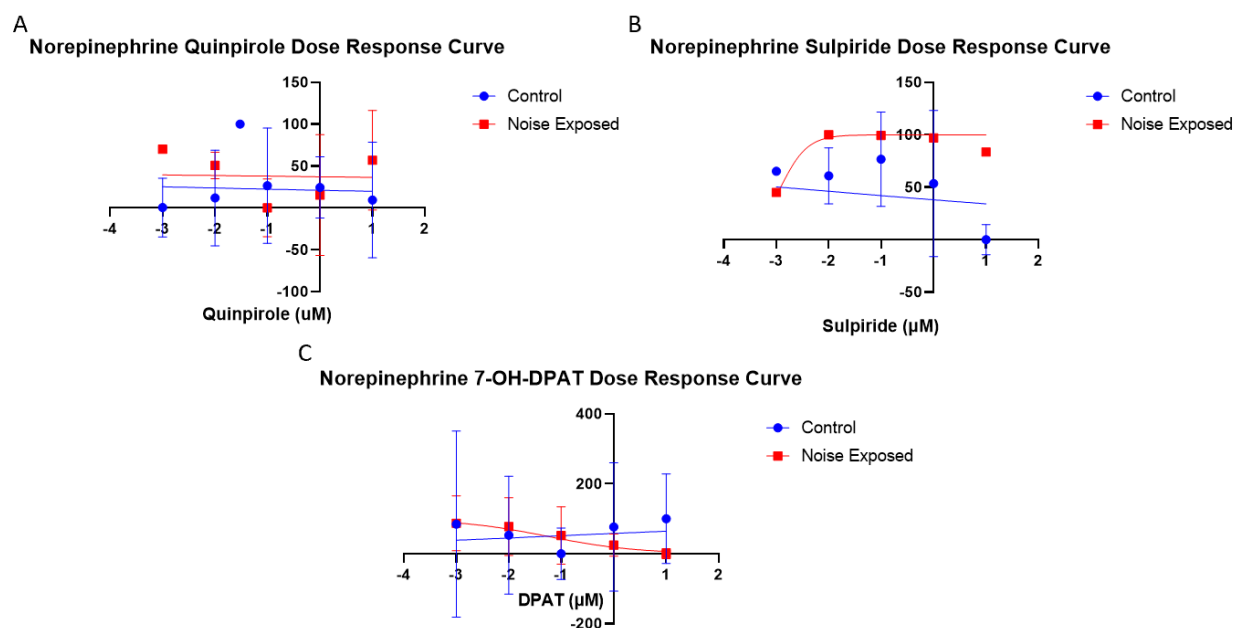
**NOISE EXPOSED NOREPINEPHRINE
DOSE RESPONSE CURVE**

Figure 41. Effects of pharmacological agents on sound exposed norepinephrine subjects. (A) Noise exposed subject effective quinpirole concentration on norepinephrine peak concentration release was 0.002954 μM. (B) Noise exposed subject effective sulpiride concentration on norepinephrine peak concentration release was 0.001026 μM. (C) Noise exposed subject effective 7-OH-DPAT concentration on norepinephrine peak concentration release was 0.1007 μM.